

UC Davis

UC Davis Previously Published Works

Title

Acute administration of diazepam or midazolam minimally alters long-term neuropathological effects in the rat brain following acute intoxication with diisopropylfluorophosphate

Permalink

<https://escholarship.org/uc/item/1nd3k8kb>

Authors

Supasai, Suangsuda
González, Eduardo A
Rowland, Douglas J
et al.

Publication Date

2020-11-01

DOI

10.1016/j.ejphar.2020.173538

Peer reviewed

Journal Pre-proof

Acute administration of diazepam or midazolam minimally alters long-term neuropathological effects in the rat brain following acute intoxication with diisopropylfluorophosphate

Suangsuda Supasai, Eduardo A. González, Douglas J. Rowland, Brad Hobson, Donald A. Bruun, Michelle A. Guignet, Sergio Soares, Vikrant Singh, Heike Wulff, Naomi Saito, Danielle J. Harvey, Pamela J. Lein

PII: S0014-2999(20)30630-0

DOI: <https://doi.org/10.1016/j.ejphar.2020.173538>

Reference: EJP 173538

To appear in: *European Journal of Pharmacology*

Received Date: 3 February 2020

Revised Date: 1 September 2020

Accepted Date: 3 September 2020

Please cite this article as: Supasai, S., González, E.A., Rowland, D.J., Hobson, B., Bruun, D.A., Guignet, M.A., Soares, S., Singh, V., Wulff, H., Saito, N., Harvey, D.J., Lein, P.J., Acute administration of diazepam or midazolam minimally alters long-term neuropathological effects in the rat brain following acute intoxication with diisopropylfluorophosphate, *European Journal of Pharmacology* (2020), doi: <https://doi.org/10.1016/j.ejphar.2020.173538>.

This is a PDF file of an article that has undergone enhancements after acceptance, such as the addition of a cover page and metadata, and formatting for readability, but it is not yet the definitive version of record. This version will undergo additional copyediting, typesetting and review before it is published in its final form, but we are providing this version to give early visibility of the article. Please note that, during the production process, errors may be discovered which could affect the content, and all legal disclaimers that apply to the journal pertain.

© 2020 Published by Elsevier B.V.



CRedit statement

S. Supasai: Methodology, Investigation, Writing-Original Draft, Visualization **E. González:** Investigation, Writing-Original Draft, Visualization **D. Rowland:** Conceptualization, Methodology, Investigation, Data Curation, Writing-Original Draft **B. Hobson:** Conceptualization, Investigation, Data Curation, Writing-Review & Editing **D. Bruun:** Investigation, Data Curation, Writing-Review & Editing, Supervision **M. Guignet:** Investigation, Writing-Review & Editing **S. Soares:** Investigation **V. Singh:** Investigation, Visualization **H. Wulff:** Methodology, Writing-Review & Editing, Supervision **N. Saito:** Formal analysis, Writing-Original Draft, Visualization **D. Harvey:** Formal analysis, Writing-Original Draft, Visualization **P. Lein:** Conceptualization, Writing-Review & Editing, Supervision, Project Administration, Funding Acquisition

1
2
3 **Acute administration of diazepam or midazolam minimally alters long-term neuropathological effects**
4 **in the rat brain following acute intoxication with diisopropylfluorophosphate**
5
6

7 Suangsuda Supasai^{a,b*}, Eduardo A. González^{a*}, Douglas J. Rowland^c, Brad Hobson^{a,c}, Donald A. Bruun^a,
8 Michelle A. Guignet^a, Sergio Soares^c, Vikrant Singh^d, Heike Wulff^d, Naomi Saito^e, Danielle J. Harvey^e, and
9 Pamela J. Lein^a
10

11 ^aDepartment of Molecular Biosciences, University of California, Davis, School of Veterinary Medicine, Davis,
12 CA 95616, USA (ssupasai@ucdavis.edu; azgonzalez@ucdavis.edu; bahobson@ucdavis.edu;
13 dabruun@ucdavis.edu; mguignet@ucdavis.edu; pjlein@ucdavis.edu); ^bDepartment of Molecular Tropical
14 Medicine and Genetics, Faculty of Tropical Medicine, Mahidol University, Bangkok 10400, Thailand
15 (suangsuda.sup@mahidol.edu); ^cCenter for Molecular and Genomic Imaging, University of California, Davis,
16 College of Engineering, Davis, CA 95616, USA (djrowland@ucdavis.edu; bahobson@ucdavis.edu;
17 srpsouares@ucdavis.edu); ^dDepartment of Pharmacology, University of California, Davis, School of Medicine,
18 Davis, CA 95616, USA (yssingh@ucdavis.edu; hwulff@ucdavis.edu); ^eDepartment of Public Health Sciences,
19 University of California, Davis, School of Medicine, Davis, CA 95616, USA (nhsaito@ucdavis.edu;
20 djharvey@ucdavis.edu).

21 *These authors contributed equally to this manuscript.
22

23 Corresponding Author: Dr. Pamela J. Lein
24 Department of Molecular Biosciences
25 University of California, Davis, School of Veterinary Medicine
26 1089 Veterinary Medicine Drive, 2009 VM3B
27 Davis, CA 95616
28 Telephone: (530) 752-1970 Fax: (530) 752-7690
29 Email: pjlein@ucdavis.edu

Abstract

Acute intoxication with organophosphorus cholinesterase inhibitors (OPs) can trigger seizures that rapidly progress to life-threatening status epilepticus. Diazepam, long considered the standard of care for treating OP-induced seizures, is being replaced by midazolam. Whether midazolam is more effective than diazepam in mitigating the persistent effects of acute OP intoxication has not been rigorously evaluated. We compared the efficacy of diazepam vs. midazolam in preventing persistent neuropathology in adult male Sprague-Dawley rats acutely intoxicated with the OP diisopropylfluorophosphate (DFP). Subjects were administered pyridostigmine bromide (0.1 mg/kg, *i.p.*) 30 min prior to injection with DFP (4 mg/kg, *s.c.*) or vehicle (saline) followed 1 min later by atropine sulfate (2 mg/kg, *i.m.*) and pralidoxime (25 mg/kg, *i.m.*), and 40 min later by diazepam (5 mg/kg, *i.p.*), midazolam (0.73 mg/kg, *i.m.*), or vehicle. At 3 and 6 months post-exposure, neurodegeneration, reactive astrogliosis, microglial activation, and oxidative stress were assessed in multiple brain regions using quantitative immunohistochemistry. Brain mineralization was evaluated by *in vivo* micro-computed tomography (micro-CT). Acute DFP intoxication caused persistent neurodegeneration, neuroinflammation, and brain mineralization. Midazolam transiently mitigated neurodegeneration, and both benzodiazepines partially protected against reactive astrogliosis in a brain region-specific manner. Neither benzodiazepine attenuated microglial activation or brain mineralization. These findings indicate that neither benzodiazepine effectively protects against persistent neuropathological changes, and suggest that midazolam is not significantly better than diazepam. Overall, this study highlights the need for improved neuroprotective strategies for treating humans in the event of a chemical emergency involving OPs.

Keywords: benzodiazepines, diazepam, micro-CT, midazolam, neuroinflammation, organophosphate neurotoxicity

54 1. Introduction

55 Organophosphorus cholinesterase inhibitors (OPs) are used as both pesticides and chemical threat agents.
56 These compounds cause hundreds of thousands of death each year as a result of accidental exposures and
57 suicides, and terrorist use of OPs remains a serious threat (Eddleston et al. 2008; Patel et al. 2012; Pereira et al.
58 2014). Inhibition of acetylcholinesterase by OPs causes cholinergic overexcitation at both central and peripheral
59 synapses (Pope, Karanth, and Liu 2005). In both humans and animals, this cholinergic crisis can trigger seizures
60 that rapidly progress to life threatening *status epilepticus* (de Araujo Furtado et al. 2012). Humans who survive
61 OP-induced *status epilepticus* often develop persistent neurological impairments, including structural brain
62 damage, cognitive deficits, and epilepsy (Chen 2012; Loh et al. 2010; Yamasue et al. 2007).

63 Current standard of care for treatment of OP poisoning includes atropine to block peripheral cholinergic
64 symptoms, an oxime to reactivate acetylcholinesterase and a benzodiazepine to terminate seizures. In the United
65 States, and other countries, midazolam is replacing diazepam as the standard of care for treating OP-induced
66 seizures. Midazolam is superior to diazepam in terminating seizures in animal models of OP-induced *status*
67 *epilepticus* (McDonough et al. 1999; McMullan et al. 2010). Based on these findings and data from the Rapid
68 Anticonvulsant Medication Prior to Arrival Trial (RAMPART) study, a double-blind clinical trial that evaluated
69 the efficacy of midazolam as an emergency anticonvulsant (Silbergleit et al. 2011, 2013), the United States
70 Food and Drug Administration determined that midazolam is superior to either diazepam or the benzodiazepine
71 lorazepam for the treatment of OP-induced seizures, largely due to increased bioavailability following *i.m.*
72 administration (FDA 2018).

73 Improved seizure termination following acute OP intoxication is thought to improve neurological outcomes
74 in exposed individuals (Jett 2016; McDonough et al. 1999). However, whether midazolam provides enhanced
75 neuroprotection relative to diazepam when administered at a delayed time after acute OP intoxication, as would
76 be the case in a mass civilian casualty or suicide attempts involving OPs, has not been rigorously evaluated.
77 Therefore, the goal of this study was to compare post-OP exposure treatment with diazepam vs. midazolam on

78 persistent neuropathology in a rat model of acute intoxication with the OP, diisopropylfluorophosphate (DFP).
79 Adult male rats acutely intoxicated with DFP exhibit persistent human-relevant neuropathology, behavioral
80 deficits, and electroencephalographic abnormalities (Deshpande et al. 2010; Guignet et al. 2020; Liang et al.
81 2017; Pouliot et al. 2016; Siso et al. 2017).

83 2. Materials and methods

84 2.1 Animals and Husbandry

85 All animals were maintained in facilities fully accredited by AAALAC International. Studies were
86 performed under protocols approved by the UC Davis Institutional Animal Care and Use Committee (IACUC
87 protocol #20165) with attention to minimizing pain and suffering. Animal experiments strictly adhered to
88 ARRIVE guidelines and the National Institutes of Health guide for the care and use of laboratory animals. Adult
89 (7-8 wk) male Sprague-Dawley rats (250-280g; Charles River Laboratories, Hollister, CA, USA) were
90 individually housed in standard plastic cages with absorbent corn cob bedding and a 12 h light/dark cycle and
91 controlled environment (22 ± 2 °C, 40-50% humidity). This species was chosen because it is a well-established
92 model for evaluating acute DFP intoxication (Pessah et al. 2016). Rodent chow (2018 Tekland global 18%
93 protein rodent diet; Envigo, Huntingdon, UK) and water were provided *ad libitum*.

94 2.2 Study design

95 The data reported here are a subset of the data generated from a single study designed to assess the efficacy
96 of diazepam and midazolam on the chronic effects of DFP-induced *status epilepticus*. All animals in the study
97 were monitored for seizure activity during the first 4 h post-DFP injection (**Fig. 1A**). In the subsequent days to
98 weeks to months, these animals were evaluated by magnetic resonance (MR) and positron emission tomography
99 (PET) imaging with each animal experiencing up to three separate imaging sessions. The data from these *in vivo*
100 imaging studies are described in a separate manuscript (Hobson et al., under review). At 3 and 6 months post-
101 exposure, the brains of a subset of these animals were also scanned using micro-computed tomography (micro-

CT) prior to euthanizing the animals to collect brains for neuropathologic analyses. For seizure monitoring, vehicle and DFP alone groups consisted of 14 animals each, while diazepam and midazolam groups consisted of 10 animals each (**Fig. 1B**). Due to the complexity of the study and limitations on the number of animals that could be imaged in a single day, animals in this study were injected across multiple days. All animals were injected in the morning, and injections on any given morning included animals from each experimental group. Following the acute seizure analysis, 3 randomly chosen animals were removed from the diazepam and midazolam groups for separate analyses not included in this study; thus 7 animals from each of these two groups were assessed for neuropathologic responses at later time points.

2.3 Pharmacokinetic Analysis of Diazepam and Midazolam

Adult male rats not injected with DFP were used to evaluate the pharmacokinetics of diazepam and midazolam. Brain and plasma concentrations were evaluated at 10 min, 1 h, 4 h, 12 h, and 24 h post-administration by ultra-performance liquid chromatography-mass spectrometry (UPLC-MS) as previously described (Ulu et al. 2016). Midazolam was analyzed by the selective reaction monitoring (SRM) transition of its positively charged quasi-molecular ion 326.08 (M+1)⁺ into product ions of 223.05, 249.04 & 291.05 m/z. Diazepam was analyzed by the SRM transition of its positively charged quasi-molecular ion 285.08 (M+1)⁺ into product ions of 227.99, 193.03 & 154.04 m/z. Adult rats were injected with either diazepam (USP grade; Hospira Inc., Lake Forest, IL, USA; 5 mg/kg, *i.p.*) or midazolam (USP grade; Hospira Inc.; 0.73 mg/kg, *i.m.*). Diazepam provided in ChemPacks is intended to be administered *i.m.* However, diazepam is known to have very poor *i.m.* bioavailability (Reddy and Reddy 2015; Ulu et al. 2016); therefore, diazepam was injected *i.p.* at 5 mg/kg, a dose that reaches therapeutic concentrations in the brain (Ulu et al. 2016). Diazepam administered *i.p.* at ≥ 5 mg/kg is used by multiple laboratories in animal models of acute OP intoxication (Auta et al. 2004; Matson et al. 2019; Zhang et al. 2017). A single autoinjector provided in the ChemPack for human use contains 10 mg midazolam, which based on allometric scaling (Nair and Jacob 2016) is approximately 0.73 mg/kg midazolam in the adult rat.

2.4 DFP Exposure and Seizure Monitoring

Animals were pretreated with pyridostigmine bromide (0.1 mg/kg *i.p.*; TCI America, Portland, USA; >98% purity), a reversible cholinesterase inhibitor, in sterile saline 30 min prior to DFP injection to minimize peripheral cholinergic symptoms (Kim et al. 1999). DFP (Sigma Chemical Company, St Louis, MO, USA) was prepared 5 min before administration in ice-cold sterile phosphate-buffered saline (PBS, 3.6 mM Na₂HPO₄, 1.4 mM NaH₂PO₄, 150 mM NaCl; pH 7.2). DFP stocks were evaluated for purity using ¹H-, ¹³C, ¹⁹F, and ³¹P-NMR methods (Gao et al. 2016) and determined to be 90 ± 7% pure. Upon arrival, DFP aliquots were stored at -80 °C, a condition that maintains chemical stability for over 1 year (Heiss et al. 2016). Rats were injected between the shoulder blades with DFP at 4 mg/kg *s.c.*, a dosing paradigm previously shown to induce *status epilepticus* (Guignet et al. 2020) in approximately 80-90% of DFP-injected animals (Gonzalez et al. 2020). Animals were then given a combined *i.m.* inner thigh injection of 2 mg/kg atropine-sulfate (Sigma; >97% purity) and 25 mg/kg pralidoxime (Sigma; >99% purity) in sterile saline (0.9% NaCl) within 1 min following DFP injection to increase survival. Atropine sulfate blocks peripheral muscarinic cholinergic receptors and pralidoxime reactivates peripheral acetylcholinesterase to minimize mortality in DFP-intoxicated rats from overstimulation of the parasympathetic nervous system (Bruun et al. 2019). Vehicle control animals were similarly treated with atropine sulfate and pralidoxime but were injected with 300 µl ice-cold sterile saline *s.c.* in place of DFP. At 40 min post-DFP exposure, animals were administered diazepam, midazolam, or an equal volume (~300 µl) of saline vehicle (*i.p.* or *i.m.*) with *i.m.* injections administered to the inner thigh of the hind leg.

Immediately following injection, all animals were monitored for seizure behavior for 4 h and the severity of seizure behavior scored using a seizure behavior scale established for use in rat models of acute OP intoxication (Deshpande et al. 2010). Two experimenters without knowledge of experimental group independently monitored animals in real-time, and scores from both experimenters were averaged for each observation. The scores for each animal were averaged over time to obtain an individual average seizure score. It has previously been demonstrated that DFP-intoxicated animal with consecutive seizure scores of ≥ 3 are experiencing *status*

150 *epilepticus* (Deshpande et al. 2010; Phelan et al. 2015). Therefore, at 40 min post-DFP administration, animals
151 with consecutive seizure scores of ≤ 3 were excluded from the study and the remaining DFP animals were
152 randomized using a random number generator into one of three groups: DFP alone, DFP + diazepam (referred
153 to as the diazepam group), or DFP + midazolam (referred to as the midazolam group). At the end of the 4 h
154 observation period animals were injected *s.c.* with 10 ml 5% dextrose in 0.9% isotonic saline (Baxter
155 International, Deerfield, IL, USA) prior to being returned to their home cages. Animals were provided access to
156 moistened chow until they resumed consumption of solid chow.

157 2.5 Micro-CT Imaging

158 At 3 and 6 months post-DFP intoxication, the brains of living animals were imaged with an Inveon Multi-
159 Modality CT scanner (Siemens Healthineers, Munich, Germany) at the University of California, Davis Center
160 for Molecular and Genomic Imaging. A subset of animals underwent micro-CT imaging at both 3 and 6 months
161 post-DFP prior to euthanasia. Sample sizes for each endpoint were determined using a two-tailed power
162 analysis, with effect size calculated using previously generated preliminary data. Animals were anesthetized
163 with isoflurane/O₂ (Piramal Healthcare, Bethlehem, PA, USA) using 2.0-3.0% isoflurane v/v to induce and 1.0-
164 2.0% isoflurane v/v to maintain anesthesia. Once anesthetized, animals were stereotactically restrained in
165 custom beds for imaging in the CT scanner. Voltage and beam current were set to 80kVp and 425 μ A,
166 respectively. A 0.5-mm aluminum filter was used to harden the beam. The detector was set to image at 4096 x
167 2048 using bin 2 with a low magnification resulting in a voxel size of 48.26 μ m. Projections were taken over
168 360° in 1° steps with a 1000-ms exposure time. Scans were reconstructed using a Feldkamp algorithm
169 (Yamamoto et al. 2007) with Shepp-Logan filter into 16 bit values. A subset of animals were imaged at both 3
170 and 6 months, generating larger sample sizes at the 3 month time point relative to the 6 month time point.

171 Images were analyzed using Amira software version 6.5.0 (Thermo Fisher Scientific). ROIs for the medial
172 and dorsolateral thalamus were drawn on previously acquired T2w images using the magnetic lasso tool (Amira
173 software). A small number of animals (0-1 per experimental group) were excluded due to image artifacts that

174 confounded quantitative analysis. All image analysis was performed completely blinded to group and time
175 point. A non-local means filter was applied to all micro-CT scans to decrease the noise in the images while
176 maintaining image clarity (Chen et al. 2018). Micro-CT scans were manually aligned with MR scans for
177 anatomical reference. An intensity threshold (intensity value ≥ 450) was applied to micro-CT scans to isolate
178 areas of mineralization as individual ROIs in the brain. Quantitative data was obtained from the automatically
179 calculated three-dimensional mineral deposits. The volumes of the medial thalamus, dorsolateral thalamus, and
180 mineralization ROIs were exported from Amira. The percent mineralization was calculated and used to conduct
181 statistical analysis. Two-dimensional cross-sections were selected from each group to enable visualization of
182 mineralization in the raw micro-CT images.

183 *2.6 Neuropathologic analyses*

184 At 3 months post-DFP, approximately half of all animals in each treatment group were randomly selected
185 for euthanasia to collect brains for neuropathologic analyses. The remaining animals were euthanized at 6
186 months post-DFP. Animals were euthanized with 4% isoflurane and transcardially perfused using a Masterflex
187 peristaltic pump (Cole Parmer, Vernon Hills, IL, USA) and 100 ml cold PBS at a flow rate of 15 ml/min.
188 FluoroJade-C staining was performed as previously described (Hobson et al. 2017). Briefly, following
189 euthanasia, brains were harvested and immediately cut into 2-mm coronal sections starting at bregma point 0
190 and post-fixed in 4% paraformaldehyde solution (Sigma) in PBS for 24 h at 4 °C. Brain sections were then
191 equilibrated in 30% w/v sucrose (Thermo Fisher Healthcare, Waltham, MA, USA) in PBS at 4 °C overnight,
192 embedded in OCT medium (Thermo Fisher Healthcare), and then cryosectioned into 10- μ m slices onto
193 Superfrost Plus slides (Thermo Fisher Healthcare). Sections were then dehydrated in 70% ethanol, incubated in
194 0.06% potassium permanganate w/v (Sigma) in distilled water for 10 min, incubated in distilled water for 2 min,
195 and incubated in 0.0001% w/v FluoroJade-C (Cat #AG325; Millipore, Billerica, MA, USA) in 0.1% v/v acetic
196 acid (Acros Organics, Geel, Belgium) in distilled water for 10 min. The FluoroJade-C solution contained a
197 1:50,000 dilution of DAPI (Invitrogen, Carlsbad, CA, USA). Slides were dried at 50 °C for 5 min, cleared in

198 chemical grade xylene (Fisher Chemical, Waltham, MA, USA) for 1 min, and mounted in 50 μ l of Permount
199 (Thermo Fisher Scientific, Waltham, MA).

200 For immunohistochemistry, sections were processed for antigen retrieval using a 10 mM sodium citrate
201 solution (pH 6.0) in distilled water for 20 min at 90 °C followed by 3 washes in PBS for 10 min. Sections were
202 then blocked in a blocking solution of PBS containing 10% w/v goat serum (Vector Laboratories, Burlingame,
203 CA, USA), 1% w/v bovine serum albumin (Sigma), and 0.03% w/v Triton X-100 (Thermo Fisher Scientific) for
204 1 h at room temperature, followed by incubation with primary antibodies in blocking solution at 4 °C overnight.
205 The primary antibodies used in this study were mouse anti-gial fibrillary acidic protein (GFAP, 1:1000, Cell
206 Signaling Technology, Danvers, MA, USA; Cat# 3670, RRID:AB_561049), rabbit anti-S100 calcium-binding
207 protein β (S100 β , 1:500, Abcam, Cambridge, UK; Cat# ab14688, RRID:AB_2184443), rabbit anti-ionized
208 calcium-binding adapter molecule 1 (IBA-1, 1:1000, Wako Laboratory Chemicals, Richmond, VA, USA; Cat#
209 019-19741, RRID:AB_839504), mouse anti-CD68 (1:200, Serotec, Hercules, CA, USA; Cat# MCA341R,
210 RRID:AB_2291300), mouse anti-NeuN (1:1000, Millipore; Cat# MAB377, RRID:AB_2298772), and rabbit
211 anti-3-nitrotyrosine (1:200, Millipore; Cat# 06-284, RRID:AB_310089). Sections were triple-washed in PBS
212 followed by 0.03% w/v Triton X-100 in PBS for 10 min and then incubated in secondary antibody in blocking
213 solution for 90 min at room temperature in complete darkness. The secondary antibody used for IBA-1 was
214 Alexa Fluor 568-conjugated goat anti-rabbit IgG (1:500, Life Technologies, Carlsbad, CA, USA; Cat# A-
215 21069, RRID:AB_2535730); for CD68, Alexa Fluor 488-conjugated goat anti-mouse IgG (1:500, Life
216 Technologies; Cat# A-11001, RRID:AB_2534069); for GFAP and NeuN, Alexa Fluor 568-conjugated goat
217 anti-mouse IgG₁ (γ 1) (1:1000, Life Technologies; Cat# A-21124, RRID:AB_2535766); and for 3-NT and
218 S100 β , Alexa Fluor 488-conjugated goat anti-rabbit IgG (1:500, Life Technologies; Cat# A-11034,
219 RRID:AB_2576217). Following incubation in secondary antibody, sections were triple-washed with PBS
220 followed by 0.03% w/v Triton X-100 in PBS for 10 min before cover slipping using ProLong Gold Antifade

221 Mountant with DAPI (Invitrogen). Negative controls were incubated with blocking buffer containing no
222 primary antibody and subsequently stained using identical protocols.

223 Fluorescent immunoreactivity was visualized using an ImageXpress XL High-Content Imaging System at
224 20X magnification (Molecular Devices, Sunnyvale, CA, USA). Images were acquired from the amygdala,
225 hippocampus (CA1, CA3, and dentate gyrus), piriform cortex, and somatosensory cortex between -3.6-mm to -
226 4.2-mm posterior to bregma and the dorsolateral thalamus between -3.0-mm to -3.6-mm posterior to bregma. A
227 rat brain atlas was used to verify that homologous bregma ranges were assessed between animals (Kruger,
228 Saporta, and Swanson 1995). A small number of animals (0-1 per experimental group) were excluded due to
229 poor image quality that confounded statistical analyses.

230 Fluorescent immunostaining was quantified as previously described (Guignet et al. 2020). Briefly, for dual
231 staining of IBA-1/CD68 and NeuN/3-nitrotyrosine, immunopositive cells were quantified in two consecutive
232 sections using the Multi-Wavelength Cell Sorting Journal within the Custom Module Editor of the MetaXpress
233 High-Content Image Acquisition and Analysis software (version 5.3, Molecular Devices) combined with a
234 Matlab script (Matlab 2014b, The Mathworks Inc., Natick, MA, USA) for Otsu's method background
235 subtraction (Otsu 1979) to identify the percentage of IBA-1 or NeuN positive cells that also expressed CD68 or
236 3-nitrotyrosine, respectively. For GFAP and S100 β staining, the area of immunofluorescence relative to the
237 total area of the ROI was analyzed separately following normalization to a background-subtracted image and
238 binarization using ImageJ (version 1.48, National Institutes of Health, Bethesda, MD, USA). Positive staining
239 was identified as fluorescence intensity that, at a minimum, was twice that of the background fluorescence
240 levels observed in negative control images. To preclude bias, image acquisition and analyses were performed by
241 a single experimenter without knowledge of exposure group or time point using automated approaches.

242 *2.7 Data and Statistical Analysis*

243 Time-weighted seizure scores were calculated for each individual animal to account for time as a variable.
244 Once a score was obtained for each individual animal, a one-way ANOVA with post-hoc Kruskal-Wallis test

was used to identify statistical differences between treatment groups. For neuropathology measures, primary outcomes of interest included the total number of FluoroJade-C stained cells, percentage of IBA-1+ cells, percentage of IBA-1+ that also co-expressed CD68, percentage of NeuN+ cells that were also immunoreactive for 3-nitrotyrosine, percentage of total cells that were NeuN+, percent area of GFAP immunoreactivity, and percent area of S100 β immunoreactivity in seven brain regions for each animal. Percent mineralization, measured by micro-CT as described above, was also available for two brain regions for each animal. Raw data points for each neuropathologic outcome are shown in supplemental Fig. 1-8.

Mixed-effect regression models, including animal-specific random effects, were used to assess differences between exposure groups by region and time point. Exploratory analysis indicated that a natural logarithmic transformation was needed for all outcomes, except percentage of NeuN+ cells, to stabilize the variance and meet the underlying assumptions of normality for the mixed effects models. Due to observed zeroes for these outcomes, all values were shifted by 0.5 prior to taking the natural logarithm. Primary factors included in the statistical analyses were exposure group (vehicle, DFP, diazepam, midazolam), brain region (which for immunohistochemistry outcomes included the thalamus, dentate gyrus, CA1, CA3, amygdala, somatosensory cortex, piriform cortex; but for micro-CT outcome included the medial thalamus, dorsolateral thalamus), and time point (3 or 6 months post-DFP). Interactions between these variables were also considered. Akaike information criterion was used for model selection to identify the best model for each outcome. Specific contrasts were constructed to test groups of interest (DFP vs. vehicle, midazolam vs. DFP, diazepam vs. DFP, and diazepam vs. midazolam) and examined using Wald tests. Within an outcome, Benjamini-Hochberg False Discovery Rate (Benjamini and Hochberg 1995) was used to correct for multiple comparisons between groups; therefore, a false discovery rate-adjusted p -value < 0.05 was considered statistically significant.

Results for all log-transformed outcomes are presented as geometric mean ratios. These ratios may be interpreted as fold changes, so that a ratio of 1.5 corresponds to a 50% increase and a ratio of 0.5 corresponds to a 50% decrease. Point estimates of the ratios and the 95% confidence intervals are presented in the figures.

When the confidence interval includes 1, there is no statistical evidence of a difference between groups. However, when the confidence interval does not include 1, the estimated effect is significant at the 5% level ($p \leq 0.05$). Results for the non-transformed outcome are presented as average differences between groups along with the 95% confidence interval. All analyses were conducted using SAS (version 9.4, SAS Institute, Inc., Cary, NC, USA), and graphics were created in R (version 3.1.0, R Core Team, Vienna, Austria).

3. Results

3.1 Benzodiazepine pharmacokinetics and effects on DFP-induced seizure behavior

Naïve adult male rats were administered diazepam (5 mg/kg, *i.p.*) or midazolam (0.73 mg/kg, *i.m.*) and euthanized at varying times post-administration to collect serum and brain samples (**Fig. 2A**). Peak concentrations of diazepam were reached within the first 1 h post-administration and were ~3-fold higher in the brain than the plasma. The brain to plasma ratio for diazepam was ~3.5. Peak concentrations of midazolam were reached at 10 min and were only slightly higher in brain tissue compared to plasma. Brain levels of midazolam remained slightly higher than plasma until 4 h when both concentrations fell below 10 nM. The greatest difference between brain and plasma concentrations of midazolam was observed at 40 min when brain levels were almost 2-fold higher than plasma levels. The brain to plasma ratio was ~1.2-2.1. Direct comparison showed higher brain concentrations of midazolam than diazepam at 10, but comparable concentrations at all other time points. Midazolam and diazepam were effectively eliminated and no longer pharmacologically active by 4 h in both brain and plasma. These pharmacokinetic profiles are consistent with prior literature for both diazepam (Fenyk-Melody et al. 2004; Ulu et al. 2016) and midazolam (Arendt et al. 1987; Miyamoto et al. 2015) and suggest that midazolam is absorbed more quickly and enters the brain more rapidly and at higher concentrations than diazepam.

To assess the relative efficacy of diazepam vs. midazolam in terminating OP-induced seizures, seizure behavior was scored in vehicle and DFP-exposed animals for 4 h post-injection using an established seizure

293 behavior scale (**Fig. 2B**). Animals demonstrated seizure behavior within 6-8 minutes following DFP
294 administration and continued seizing for the duration of the 4 h monitoring period. For the first 2.5 h, DFP
295 animals maintained severe seizure scores (≥ 3) that then began to decline. Animals treated with diazepam at 40
296 min post-DFP intoxication showed markedly reduced seizure scores within 20 min of diazepam administration.
297 For the last 2 h of seizure monitoring, diazepam-treated animals showed seizure scores of ~ 2 , which are below
298 the threshold seizure score thought to be consistent with *status epilepticus* (Deshpande et al. 2010; Phelan et al.
299 2015). Similarly, midazolam-treated animals showed decreased seizure behavior within 20 min and also
300 maintained seizure scores of ~ 2 through the rest of the seizure monitoring period. Although both diazepam and
301 midazolam attenuated seizure behavior, neither benzodiazepine reduced seizure behavior to baseline levels
302 observed in vehicle control animals.

303 Seizure scores collected at individual time points post-injection for each individual animal were averaged to
304 obtain an average seizure score over the 4 h period for that animal. Average seizure scores for each group
305 confirmed that DFP animals experienced significant seizure behavior, as previous studies indicate that
306 prolonged seizure scores of ≥ 3 are consistent with *status epilepticus* (Deshpande et al. 2010; Phelan et al.
307 2015). These data also confirmed that post-exposure treatment with either diazepam or midazolam significantly
308 attenuated DFP-induced seizure behavior but did not return behavior to baseline levels. Importantly, there were
309 no significant differences in average seizure scores between DFP + diazepam and DFP + midazolam animals.

310 3.2 Neurodegeneration is transiently reduced by midazolam

311 FluoroJade-C staining was used to visualize degenerating or recently degenerated neurons (Schmued et al.
312 2005) in multiple brain regions, including the CA1, CA3 and dentate gyrus of the hippocampus, the amygdala,
313 piriform and somatosensory cortex, and the thalamus at 3 and 6 months after acute intoxication with DFP (**Fig.**
314 **3A**). The number of FluoroJade-C-labeled cells differed between groups by time point ($F(3, 204)=3.82, P=0.01$)
315 but not by brain region. Therefore, estimates of group differences at each time point were averaged across brain
316 regions. At both 3 ($t(204)=3.78, P=0.0002$) and 6 months ($t(204)=6.44, P<0.0001$), DFP animals had a

317 significantly increased number of FluoroJade-C-labeled cells relative to vehicle animals in all brain regions
318 (**Fig. 3B**). While there was a trend towards significance at 3 months, diazepam-treated DFP animals did not
319 have significantly decreased FluoroJade-C labeling at 3 or 6 months. At 3 months, midazolam significantly
320 decreased FluoroJade-C labeling ($t(204)=-2.38$, $P=0.018$); however, by 6 months, there was no significant
321 difference between DFP animals that did not receive benzodiazepine vs. DFP animals that were treated with
322 midazolam. The difference between DFP and vehicle animals remained significant after false discovery rate
323 correction. There were no differences between diazepam and midazolam-treated DFP animals at either time
324 point.

325 *3.3 Midazolam reduces reactive astrogliosis in more brain regions than diazepam*

326 Reactive astrogliosis was measured using GFAP (**Fig. 4A**) and S100 β (**Fig. 5A**) immunoreactivity to
327 capture populations of astrocytes that uniquely express one of these two biomarkers (reviewed in Holst et al.
328 2019). The difference between groups in percent area of GFAP immunoreactivity varied by brain region
329 ($F(18,188)=4.04$, $P<0.0001$) but not by time point. Thus, estimates of group differences by brain region were
330 averaged across time points. The percent area of GFAP immunoreactivity was significantly increased in DFP
331 compared to vehicle animals in all seven brain regions examined (**Fig. 4B**, $P<0.005$). In the initial mixed-effect
332 comparison, DFP animals treated with diazepam had significantly reduced GFAP expression in the
333 hippocampal CA1 subregion ($t(188)=-2.11$, $P=0.036$) and somatosensory cortex ($t(188)=-2.04$, $P=0.043$)
334 compared to DFP animals that did not receive any benzodiazepine, but these differences did not remain
335 significant after false discovery rate correction. Treatment with midazolam significantly decreased GFAP
336 expression in the CA1 ($t(188)=-4.01$, $P<0.0001$), CA3 ($t(188)=-2.37$, $P=0.019$), and dentate gyrus ($t(188)=-$
337 2.48 , $P=0.014$) subregions of the hippocampus, as well as in the somatosensory cortex ($t(188)=-4.41$, $P<0.0001$)
338 and thalamus ($t(188)=-2.36$, $P=0.019$) compared to DFP animals that did not receive any benzodiazepine, and
339 these all remained significant after false discovery rate correction. There were no differences between diazepam
340 or midazolam-treated DFP animals.

The percent area of S100 β immunoreactivity also differed by brain region ($F(18,182)=5.95$, $P<0.0001$) but not by time point. The percent area of S100 β immunoreactivity was significantly greater in DFP than vehicle animals in all brain regions studied, although the difference in the hippocampal CA3 and dentate gyrus did not remain significant after false discovery rate correction (**Fig. 5B**). Diazepam decreased S100 β expression in the hippocampal CA1 ($t(182)=-2.14$, $P=0.033$), dentate gyrus ($t(182)=-2.86$, $P=0.0047$) and somatosensory cortex ($t(182)=-3.16$, $P=0.0018$), although the difference in the CA1 did not remain significant after false discovery rate correction. Midazolam decreased S100 β expression in the hippocampal CA1 ($t(182)=-2.66$, $P=0.0086$), somatosensory cortex ($t(182)=-4.56$, $P<0.0001$), and thalamus ($t(182)=-5.12$, $P<0.0001$), all of which remained significant after false discovery rate correction. DFP animals treated with diazepam had significantly increased S100 β expression in the thalamus compared to DFP animals treated with midazolam ($t(182)=4.55$, $P<0.0001$), which remained significant after false discovery rate correction.

3.4 Neither midazolam nor diazepam reduces microglial activation

Microglial activation was measured as the percentage of cells within the field that were immunopositive for IBA-1 and by the percentage of IBA-1 immunopositive cells that were phagocytic, as identified by co-labelling for CD68 (**Fig. 6A**). The differences between groups in percentage of IBA-1 immunopositive cells did not differ by brain region or time point (**Fig. 6B**). DFP animals had a higher percentage of IBA-1 immunopositive cells than vehicle animals ($t(32)=2.12$, $P=0.04$), but this difference did not remain significant after false discovery rate correction. There was a significant difference between groups in the percentage of IBA-1 immunopositive cells that co-expressed CD68 ($F(3,32)=9.95$, $P<0.0001$), and this difference was similar across brain regions and time points. DFP animals showed an increased percentage of CD68-labeled IBA-1 immunopositive cells compared to vehicle animals ($t(32)=5.34$, $P<0.0001$) that remained significant after false discovery rate correction. However, there were no differences between DFP animals treated with diazepam or midazolam compared to DFP animals not treated with any benzodiazepine. Furthermore, there was no difference between diazepam and midazolam-treated DFP animals.

365 3.5 DFP-induced oxidative stress returns to baseline levels by 6 months post-intoxication

366 Previous studies have shown that biomarkers of oxidative stress increase in the rat brain following acute
367 DFP intoxication (Pearson and Patel 2016) and persist up to 2 months post-intoxication (Guignet et al. 2020).
368 Here, co-localization of 3-nitrotyrosine and NeuN immunoreactivity was used to determine whether oxidative
369 stress in neurons persists at 3 and 6 months post-DFP exposure. The expression of 3-nitrotyrosine was
370 normalized to the number of neurons (NeuN) (**Fig. 7A**). While there were no significant differences in the
371 number of NeuN+ cells between treatment groups, there was a trend towards decreased neuronal numbers in
372 DFP animals relative to vehicle (**Fig. 7B**). Similarly, there was no significant difference between groups in the
373 number of cells co-labeled for 3-nitrotyrosine and NeuN, but there was a strong trend towards increased
374 expression in DFP animals relative to vehicle.

375 3.6 Diazepam is more effective than midazolam in mitigating mineralization in the medial thalamus

376 Acute OP intoxication produces pronounced calcium dysregulation (reviewed in Deshpande, Blair, Phillips,
377 et al. 2016), thus, we used *in vivo* micro-CT imaging to monitor the formation and presence of mineral
378 inclusions in the medial and dorsolateral thalamus of DFP-intoxicated rats at 3 and 6 months (**Fig. 8A and 8B**).
379 Two-dimensional cross-sections of microCT images (color) overlaid on anatomical MRI images (grayscale)
380 show focal areas of mineralization in the 48 micron thick slice (**Fig. 8A**). The difference in percent
381 mineralization between groups, which was quantified from three-dimensional reconstructions of mineralized
382 areas, varied by both time point and brain region. DFP animals had a higher percent mineralization than vehicle
383 animals at both time points and both brain regions (**Fig. 8C**, $P < 0.05$). Diazepam decreased mineralization in the
384 medial, but not dorsolateral, thalamus at both 3 ($t(50) = -2.97$, $P = 0.0045$) and 6 months ($t(50) = -2.44$, $P = 0.018$).
385 Midazolam decreased mineralization in the medial thalamus at 6, but not 3, months ($t(50) = -2.41$, $P = 0.02$);
386 midazolam had no significant protective effect on mineralization in the dorsolateral thalamus at either time
387 point. Diazepam-treated DFP animals had a lower percent of mineralization than midazolam-treated DFP

388 animals in the medial thalamus ($t(50)=-2.76$, $P=0.0081$) at 3 months but not at 6 months. All differences
389 remained significant after false discovery rate correction.

391 4. Discussion

392 Previous work has demonstrated that DFP-induced *status epilepticus* triggers neuroinflammation in the
393 days to weeks following acute intoxication (Flannery et al. 2016; Li et al. 2015; Liu et al. 2012; Wu, Kuruba,
394 and Reddy 2018). Here we show that robust neuroinflammation persists at 3 and 6 months post-DFP
395 intoxication, as evidenced by increased expression of IBA-1, CD68, GFAP, and S100 β . We previously
396 demonstrated that neuroinflammation measured by IBA-1 immunoreactivity was more severe at 1 month than 2
397 months post-DFP (Guignet et al. 2020; Siso et al. 2017). The present findings demonstrate that IBA-1
398 immunoreactivity does not decrease with time but rather remains elevated in the brain at least until 6 months
399 post-DFP. While IBA-1 is a marker of microglia, it also labels monocytes and macrophages (Ito et al. 1998),
400 which may migrate from the periphery to contribute to the inflammatory response in the brain. Thus, the
401 elevated IBA-1 immunoreactivity we observe at 3 and 6 months post-exposure may indicate not only
402 microgliosis, but also infiltration of peripheral immune cells into the brain. In contrast, reactive astrogliosis is
403 relatively consistent in the brain with limited temporal or regional variability up to 2 months post-exposure
404 (Guignet et al. 2020; Siso et al. 2017), peaking later than either microgliosis or neuronal degeneration (Siso et
405 al. 2017). Consistent with these earlier reports, we saw relatively uniform GFAP reactivity across all seven
406 brain regions that persisted at 3 and 6 months post-DFP exposure.

407 While our earlier study found that DFP-induced neurodegeneration declined to background levels by 2
408 months post-exposure (Siso et al. 2017), here, we observed significant neurodegeneration at 3 and 6 months
409 post-exposure in all seven brain regions examined. The increase in neurodegeneration at 3 and 6 months may
410 contribute to the persistent microgliosis observed at these later time points. The delayed neurodegeneration
411 observed in the DFP-intoxicated brain may be due in part to spontaneous recurrent seizures that develop in

412 >80% of animals that survive OP-induced *status epilepticus* (de Araujo Furtado et al. 2010; Guignet et al.
413 2020). Given the extensive literature implicating neuroinflammation in the pathogenesis of impaired cognition
414 and epilepsy (reviewed in Guignet and Lein 2018), our data suggest a feed-forward model in which
415 neuroinflammation promotes persistent electrographic and neurological deficits in the months following acute
416 OP intoxication (Flannery et al. 2016; Guignet et al. 2020), which in turn sustains the neuroinflammatory
417 response. While neuroinflammation has yet to be causally linked to either the chronic cognitive deficits or
418 electrographic abnormalities associated with acute OP intoxication, several studies have shown that anti-
419 inflammatory compounds protect against some aspects of OP-induced neurological damage (Finkelstein et al.
420 2012; Li et al. 2012; Pan et al. 2015; Piermartiri et al. 2015). These observations, together with our findings of
421 persistent neuroinflammation, support neuroimmune modulation as a viable therapeutic strategy for protecting
422 against OP-induced persistent neurological consequences.

423 Robust increases in the expression of biomarkers of oxidative stress have been documented in the hours and
424 days immediately following acute DFP intoxication (Chaubey et al. 2019; Liang et al. 2017; López-Granero et
425 al. 2013; Zaja-Milatovic et al. 2009). We previously observed oxidative stress in the rat brain at both 1 and 2
426 months post-DFP intoxication (Guignet et al. 2020). However, here, we observed low to negligible levels of 3-
427 NT at 3 and 6 months post-exposure. The absence of oxidative stress despite persistent neuroinflammation is
428 surprising given the typically close relationship between these activities (reviewed in Guignet and Lein 2018).
429 One caveat of our study is that only one biomarker of oxidative stress was used, thus, follow-up studies
430 evaluating additional markers of oxidative stress at these later time points would be useful to further understand
431 the temporal profile of oxidative damage in this model.

432 A novel finding of this study was the significant mineralization in the thalamus of DFP-intoxicated animals
433 detected by micro-CT imaging at both 3 and 6 months post-exposure. While this technique does not identify the
434 chemical composition of mineral deposits, calcium is a primary constituent of mineral deposits detected by
435 micro-CT and calcium deposits frequently occur in the thalamus (Valdes Hernandez Mdel et al. 2012).

436 Additionally, *status epilepticus* and the associated glutamatergic excitotoxicity have been shown to increase
437 intracellular calcium concentrations to pathogenic levels (reviewed in Deshpande, Blair, Phillips, et al. 2016;
438 Maher et al. 2018). Although calcium is likely a primary component of the mineral deposits we observed, iron,
439 copper, and manganese have also been identified as significant components of mineralized areas in damaged
440 brain tissue (Valdes Hernandez Mdel et al. 2012). Follow-up studies evaluating the chemical composition of
441 mineral deposits are needed to better understand this aspect of the chronic pathophysiology of acute DFP
442 intoxication.

443 To the best of our knowledge, this is the first report of mineral deposits in the brain of acute OP-intoxicated
444 animals. Although the functional consequences of cerebral mineral deposits are poorly understood, calcium
445 dyshomeostasis is associated with altered neuronal activity and impaired cognition (Kirkland, Sarlo, and Holton
446 2018; Lerdkrai et al. 2018; Muller et al. 2018). Additionally, mineral deposits occur naturally in the aging brain,
447 contributing to age-related cognitive decline (reviewed in Youssef et al. 2016). The presence of persistent
448 mineral deposits in the brains of DFP-intoxicated animals suggest the intriguing possibility that acute DFP
449 intoxication accelerates the onset and/or progression of aging phenotypes. Our findings also support the
450 possibility that stabilizing calcium levels will protect against chronic OP-induced neuropathology. Indeed, the
451 calcium-stabilizing compound dantrolene was recently shown to protect against OP-induced neurodegeneration
452 at 2 d post-intoxication (Deshpande, Blair, Huang, et al. 2016). While additional research is required to evaluate
453 the causal relationship between calcium dysregulation and neurological function following acute OP
454 intoxication, our data suggest that monitoring mineralization by micro-CT may be a non-invasive, longitudinal
455 biomarker of neuropathology.

456 Our results demonstrate that diazepam and midazolam partially mitigate the long-term neuropathological
457 consequences of acute DFP intoxication. While these benzodiazepines reduced acute seizure behavior to
458 comparable levels, at 3 months post-DFP exposure, midazolam conferred protection against neurodegeneration
459 whereas diazepam did not, but diazepam protected against mineralization while midazolam did not. However,

460 neither drug significantly reduced neurodegeneration at 6 months, and both were only partially protective
461 against mineralization at 6 months. Neither midazolam nor diazepam reduced microglial activation at 3 or 6
462 months post-DFP. While both compounds reduced reactive astrogliosis, midazolam reduced both GFAP and
463 S100 β immunoreactivity, whereas diazepam only reduced S100 β expression. Additionally, midazolam
464 protected against neuroinflammation in more brain regions than diazepam. Interestingly, neither benzodiazepine
465 was effective in protecting against DFP-induced astrogliosis in the piriform cortex or amygdala. GABA_A
466 receptor subunits are heterogeneously distributed in the brain (Mennini and Gobbi 1990; Nutt 2006); thus,
467 regional differences in the GABA_A subunit composition likely contribute to the region-specific neuroprotection
468 observed in the brain of DFP animals treated with benzodiazepines. The α 5 subunit is reported to play an
469 important role in the inhibitory response to benzodiazepines (Etherington et al. 2017), and expression of the α 5
470 subunit is very low in the amygdala and piriform cortex (Pirker et al. 2000). While benzodiazepines bind
471 primarily to synaptic GABA_A receptors, the α 5 subunit is highly expressed in both synaptic and extrasynaptic
472 receptors. Should this subunit play a role in neuroprotection following OP intoxication, compounds that target
473 extrasynaptic GABA_A receptors, such as neurosteroids, may confer additional neuroprotection.

474 Benzodiazepine administration within 10 min after acute DFP intoxication has been reported to protect the
475 brain against acute neuropathology (Kuruba, Wu, and Reddy 2018; Wu, Kuruba, and Reddy 2018). However,
476 delaying benzodiazepine treatment more than 10 min post-exposure offers only partial neuroprotection in the
477 days following OP intoxication (Gilat et al. 2005; Kuruba, Wu, and Reddy 2018; Spampanato et al. 2019; Wu,
478 Kuruba, and Reddy 2018). Our data extend these previous studies by demonstrating that delayed administration
479 of benzodiazepines also fails to provide neuroprotection at months post-exposure, and by showing that neither
480 benzodiazepine provides a neuroprotective advantage relative to the other. Unfortunately, many victims of acute
481 OP intoxication will not receive immediate medical attention (Jett and Spriggs 2020). This sobering fact
482 coupled with our findings that neither diazepam nor midazolam offers complete neuroprotection at 3 or 6

months post-DFP intoxication when administered at 40 min post-OP intoxication suggest the urgent need for neuroprotective therapeutics to complement the current standard of care.

Acknowledgements

We thank Dr. Suzette Smiley-Jewell (UC Davis CounterACT Center) for her assistance in editing this manuscript. This work was supported by the CounterACT Program, National Institutes of Health (NIH) Office of the Director and the National Institute of Neurological Disorders and Stroke (NINDS) [grant number U54 NS079202], predoctoral fellowships to E.A.G from the NINDS [grant number F31 NS110522], the NIH Initiative for Maximizing Student Development [grant number R25 GM5676520], and the ARCS Foundation, and predoctoral fellowships to B.A.H. and M.G. from the National Institute of General Medical Sciences [grant number T32 GM099608] and the David and Dana Loury Foundation. This project used core facilities supported by the UC Davis MIND Institute Intellectual and Developmental Disabilities Research Center (U54 HD079125). The sponsors were not involved in the study design, in the collection, analysis, or interpretation of data, in the writing of the report, or in the decision to submit the paper for publication.

CRedit statement

S. Supasai: Methodology, Investigation, Writing-Original Draft, Visualization **E. González:** Investigation, Writing-Original Draft, Visualization **D. Rowland:** Conceptualization, Methodology, Investigation, Data Curation, Writing-Original Draft **B. Hobson:** Conceptualization, Investigation, Data Curation, Writing-Review & Editing **D. Bruun:** Investigation, Data Curation, Writing-Review & Editing, Supervision **M. Guignet:** Investigation, Writing-Review & Editing **S. Soares:** Investigation **V. Singh:** Investigation, Visualization **H. Wulff:** Methodology, Writing-Review & Editing, Supervision **N. Saito:** Formal analysis, Writing-Original

Draft, Visualization **D. Harvey:** Formal analysis, Writing-Original Draft, Visualization **P. Lein:** Conceptualization, Writing-Review & Editing, Supervision, Project Administration, Funding Acquisition

References

- Arendt, R. M., D. J. Greenblatt, D. C. Liebisch, M. D. Luu, and S. M. Paul. 1987. 'Determinants of benzodiazepine brain uptake: lipophilicity versus binding affinity', *Psychopharmacology (Berl)*, 93: 72-6.
- Auta, J., E. Costa, J. Davis, and A. Guidotti. 2004. 'Imidazenil: a potent and safe protective agent against diisopropyl fluorophosphate toxicity', *Neuropharmacology*, 46: 397-403.
- Benjamini, Yoav, and Yoel Hochberg. 1995. 'Controlling the False Discovery Rate: A Practical and Powerful Approach to Multiple Testing', *Journal of the Royal Statistical Society. Series B (Methodological)*, 57: 289-300.
- Bruun, D. A., M. Guignet, D. J. Harvey, and P. J. Lein. 2019. 'Pretreatment with pyridostigmine bromide has no effect on seizure behavior or 24 hour survival in the rat model of acute diisopropylfluorophosphate intoxication', *Neurotoxicology*, 73: 81-84.
- Chaubey, Kalyani, Syed Imteyaz Alam, Chandra Kant Waghmare, Lokendra Singh, Nalini Srivastava, and Bijoy K. Bhattacharya. 2019. 'Differential proteome analysis of rat plasma after diisopropyl fluorophosphate (DFP) intoxication, a surrogate of nerve agent sarin', *Chemico-Biological Interactions*, 298: 66-71.
- Chen, K. C., A. Arad, Z. M. Song, and D. Croaker. 2018. 'High-definition neural visualization of rodent brain using micro-CT scanning and non-local-means processing', *BMC Med Imaging*, 18: 38.
- Chen, Y. 2012. 'Organophosphate-induced brain damage: mechanisms, neuropsychiatric and neurological consequences, and potential therapeutic strategies', *Neurotoxicology*, 33: 391-400.
- de Araujo Furtado, M., L. A. Lumley, C. Robison, L. C. Tong, S. Lichtenstein, and D. L. Yourick. 2010. 'Spontaneous recurrent seizures after status epilepticus induced by soman in Sprague-Dawley rats', *Epilepsia*, 51: 1503-10.
- de Araujo Furtado, M., F. Rossetti, S. Chanda, and D. Yourick. 2012. 'Exposure to nerve agents: from status epilepticus to neuroinflammation, brain damage, neurogenesis and epilepsy', *Neurotoxicology*, 33: 1476-90.
- Deshpande, L. S., D. S. Carter, R. E. Blair, and R. J. DeLorenzo. 2010. 'Development of a prolonged calcium plateau in hippocampal neurons in rats surviving status epilepticus induced by the organophosphate diisopropylfluorophosphate', *Toxicol Sci*, 116: 623-31.
- Deshpande, Laxmikant S., Robert E. Blair, Beverly A. Huang, Kristin F. Phillips, and Robert J. DeLorenzo. 2016. 'Pharmacological blockade of the calcium plateau provides neuroprotection following organophosphate paraoxon induced status epilepticus in rats', *Neurotoxicology and teratology*, 56: 81-86.
- Deshpande, Laxmikant S., Robert E. Blair, Kristin F. Phillips, and Robert J. DeLorenzo. 2016. 'Role of the calcium plateau in neuronal injury and behavioral morbidities following organophosphate intoxication', *Annals of the New York Academy of Sciences*, 1374: 176-83.
- Eddleston, M., N. A. Buckley, P. Eyer, and A. H. Dawson. 2008. 'Management of acute organophosphorus pesticide poisoning', *Lancet*, 371: 597-607.
- Etherington, Lori-An, Balázs Mihalik, Adrienn Pálvölgyi, István Ling, Katalin Pallagi, Szabolcs Kertész, Péter Varga, Ben G. Gunn, Adam R. Brown, Matthew R. Livesey, Olivia Monteiro, Delia Belelli, József

- 549 Barkóczy, Michael Spedding, István Gacsályi, Ferenc A. Antoni, and Jeremy J. Lambert. 2017.
550 'Selective inhibition of extra-synaptic α 5-GABAA receptors by S44819, a new therapeutic agent',
551 *Neuropharmacology*, 125: 353-64.
- 552 FDA. 2018. 'Center For Drug Evaluation And Research- Midazolam Review', *Food and Drug*
553 *Administration*, Application 209566Orig1s000.
- 554 Fenyk-Melody, J. E., X. Shen, Q. Peng, W. Pikounis, L. Colwell, J. Pivnichny, L. C. Anderson, and C. S.
555 Tamvakopoulos. 2004. 'Comparison of the effects of perfusion in determining brain penetration
556 (brain-to-plasma ratios) of small molecules in rats', *Comp Med*, 54: 378-81.
- 557 Finkelstein, Arseny, Gilad Kunis, Tamara Berkutzki, Ayal Ronen, Amir Krivoy, Eti Yoles, David Last, Yael
558 Mardor, Kerry Van Shura, Emylee McFarland, Benedict A. Capacio, Claire Eisner, Mary Gonzales,
559 Danise Gregorowicz, Arik Eisenkraft, John H. McDonough, and Michal Schwartz. 2012.
560 'Immunomodulation by poly-YE reduces organophosphate-induced brain damage', *Brain,*
561 *Behavior, and Immunity*, 26: 159-69.
- 562 Flannery, B. M., D. A. Bruun, D. J. Rowland, C. N. Banks, A. T. Austin, D. L. Kukis, Y. Li, B. D. Ford, D. J.
563 Tancredi, J. L. Silverman, S. R. Cherry, and P. J. Lein. 2016. 'Persistent neuroinflammation and
564 cognitive impairment in a rat model of acute diisopropylfluorophosphate intoxication', *J*
565 *Neuroinflammation*, 13: 267.
- 566 Gao, J., S. X. Naughton, H. Wulff, V. Singh, W. D. Beck, J. Magrane, B. Thomas, N. A. Kaidery, C. M.
567 Hernandez, and A. V. Terry, Jr. 2016. 'Diisopropylfluorophosphate Impairs the Transport of
568 Membrane-Bound Organelles in Rat Cortical Axons', *J Pharmacol Exp Ther*, 356: 645-55.
- 569 Gilat, E., T. Kadar, A. Levy, I. Rabinovitz, G. Cohen, Y. Kapon, R. Sahar, and R. Brandeis. 2005.
570 'Anticonvulsant treatment of sarin-induced seizures with nasal midazolam: An electrographic,
571 behavioral, and histological study in freely moving rats', *Toxicol Appl Pharmacol*, 209: 74-85.
- 572 Gonzalez, E. A., A. C. Rindy, M. A. Guignet, J. J. Calsbeek, D. A. Bruun, A. Dhir, P. Andrew, N. Saito, D. J.
573 Rowland, D. J. Harvey, M. A. Rogawski, and P. J. Lein. 2020. 'The chemical convulsant
574 diisopropylfluorophosphate (DFP) causes persistent neuropathology in adult male rats
575 independent of seizure activity', *Arch Toxicol*.
- 576 Guignet, M., K. Dhakal, B. M. Flannery, B. A. Hobson, D. Zolkowska, A. Dhir, D. A. Bruun, S. Li, A. Wahab, D. J.
577 Harvey, J. L. Silverman, M. A. Rogawski, and P. J. Lein. 2020. 'Persistent behavior deficits,
578 neuroinflammation, and oxidative stress in a rat model of acute organophosphate intoxication',
579 *Neurobiol Dis*, 133: 104431.
- 580 Guignet, M., and P. J. Lein. 2018. 'Organophosphates.' in M. Aschner and L. G. Costa (eds.), *Advances in*
581 *Neurotoxicology: Role of Inflammation in Environmental Neurotoxicity*. (Elsevier: Oxford, UK).
- 582 Heiss, Derik R., Donald W. Zehnder, David A. Jett, Gennady E. Platoff, David T. Yeung, and Bobby N.
583 Brewer. 2016. 'Synthesis and Storage Stability of Diisopropylfluorophosphate', *Journal of*
584 *Chemistry*, 2016: 5.
- 585 Hobson, B. A., D. J. Rowland, S. Supasai, D. J. Harvey, P. J. Lein, and J. R. Garbow. 2017. 'A magnetic
586 resonance imaging study of early brain injury in a rat model of acute DFP intoxication',
587 *Neurotoxicology*.
- 588 Holst, C. B., C. B. Brochner, K. Vitting-Seerup, and K. Møllgaard. 2019. 'Astroglialogenesis in human fetal
589 brain: complex spatiotemporal immunoreactivity patterns of GFAP, S100, AQP4 and YKL-40', *J*
590 *Anat*.
- 591 Ito, D., Y. Imai, K. Ohsawa, K. Nakajima, Y. Fukuuchi, and S. Kohsaka. 1998. 'Microglia-specific localisation
592 of a novel calcium binding protein, Iba1', *Brain Res Mol Brain Res*, 57: 1-9.
- 593 Jett, D. A., and S. M. Spriggs. 2020. 'Translational research on chemical nerve agents', *Neurobiol Dis*, 133:
594 104335.

- Jett, David A. 2016. 'The NIH Countermeasures Against Chemical Threats Program: overview and special challenges', *Annals of the New York Academy of Sciences*, 1374: 5-9.
- Kim, Y. B., G. H. Hur, S. Shin, D. E. Sok, J. K. Kang, and Y. S. Lee. 1999. 'Organophosphate-induced brain injuries: delayed apoptosis mediated by nitric oxide', *Environ Toxicol Pharmacol*, 7: 147-52.
- Kirkland, Anna E., Gabrielle L. Sarlo, and Kathleen F. Holton. 2018. 'The Role of Magnesium in Neurological Disorders', *Nutrients*, 10: 730.
- Kruger, L., S. Saporta, and L.W. Swanson. 1995. *Photographic atlas of the rat brain: the cell and fiber architecture illustrated in three planes with stereotaxic coordinates*. (Cambridge University Press: Cambridge).
- Kuruba, Ramkumar, Xin Wu, and Doodipala Samba Reddy. 2018. 'Benzodiazepine-refractory status epilepticus, neuroinflammation, and interneuron neurodegeneration after acute organophosphate intoxication', *Biochimica et Biophysica Acta (BBA) - Molecular Basis of Disease*, 1864: 2845-58.
- Lerdkrai, C., N. Asavapanumas, B. Brawek, Y. Kovalchuk, N. Mojtahedi, M. Olmedillas Del Moral, and O. Garaschuk. 2018. 'Intracellular Ca(2+) stores control in vivo neuronal hyperactivity in a mouse model of Alzheimer's disease', *Proc Natl Acad Sci U S A*, 115: E1279-e88.
- Li, Y., P. J. Lein, G. D. Ford, C. Liu, K. C. Stovall, T. E. White, D. A. Bruun, T. Tewolde, A. S. Gates, T. J. Distel, M. C. Surles-Zeigler, and B. D. Ford. 2015. 'Neuregulin-1 inhibits neuroinflammatory responses in a rat model of organophosphate-nerve agent-induced delayed neuronal injury', *J Neuroinflammation*, 12: 64.
- Li, Yonggang, Pamela J. Lein, Cuimei Liu, Donald A. Bruun, Cecilia Giulivi, Gregory D. Ford, Teclmichael Tewolde, Catherine Ross-Inta, and Byron D. Ford. 2012. 'Neuregulin-1 is neuroprotective in a rat model of organophosphate-induced delayed neuronal injury', *Toxicol Appl Pharmacol*, 262: 194-204.
- Liang, L. P., J. N. Pearson-Smith, J. Huang, P. McElroy, B. J. Day, and M. Patel. 2017. 'Neuroprotective Effects of AEOL10150 in a Rat Organophosphate Model', *Toxicol Sci*.
- Liu, C., Y. Li, P. J. Lein, and B. D. Ford. 2012. 'Spatiotemporal patterns of GFAP upregulation in rat brain following acute intoxication with diisopropylfluorophosphate (DFP)', *Curr Neurobiol*, 3: 90-97.
- Loh, Yince, Margaret M. Swanberg, M. Victoria Ingram, and Jonathan Newmark. 2010. 'Case report: Long-term cognitive sequelae of sarin exposure', *Neurotoxicology*, 31: 244-46.
- López-Granero, Caridad, Fernando Cañadas, Diana Cardona, Yingchun Yu, Estela Giménez, Rafael Lozano, Daiana Silva Avila, Michael Aschner, and Fernando Sánchez-Santed. 2013. 'Chlorpyrifos-, diisopropylphosphorofluoridate-, and parathion-induced behavioral and oxidative stress effects: are they mediated by analogous mechanisms of action?', *Toxicol Sci*, 131: 206-16.
- Maher, P., K. van Leyen, P. N. Dey, B. Honrath, A. Dolga, and A. Methner. 2018. 'The role of Ca(2+) in cell death caused by oxidative glutamate toxicity and ferroptosis', *Cell Calcium*, 70: 47-55.
- Matson, L., E. Dunn, K. Haines, S. Miller-Smith, R. Lee-Stubbs, K. Whitten, C. Ardinger, H. McCarren, and J. McDonough. 2019. 'Evaluation of first-line anticonvulsants to treat nerve agent-induced seizures and prevent neuropathology in adult and pediatric rats', *Neurotoxicology*, 74: 203-08.
- McDonough, J. H., Jr., J. McMonagle, T. Copeland, D. Zoefel, and T. M. Shih. 1999. 'Comparative evaluation of benzodiazepines for control of soman-induced seizures', *Arch Toxicol*, 73: 473-8.
- McMullan, J., C. Sasson, A. Pancioli, and R. Silbergleit. 2010. 'Midazolam versus diazepam for the treatment of status epilepticus in children and young adults: a meta-analysis', *Acad Emerg Med*, 17: 575-82.
- Mennini, T., and M. Gobbi. 1990. 'Regional distribution of low-affinity GABA receptors coupled to benzodiazepine receptor subtypes in rat brain: an autoradiographic evaluation', *Eur J Pharmacol*, 189: 143-8.

- 641 Miyamoto, H., S. Matsueda, A. Moritsuka, K. Shimokawa, H. Hirata, M. Nakashima, H. Sasaki, S. Fumoto,
642 and K. Nishida. 2015. 'Evaluation of hypothermia on the in vitro metabolism and binding and in
643 vivo disposition of midazolam in rats', *Biopharm Drug Dispos*, 36: 481-9.
- 644 Muller, M., U. Ahumada-Castro, M. Sanhueza, C. Gonzalez-Billault, F. A. Court, and C. Cardenas. 2018.
645 'Mitochondria and Calcium Regulation as Basis of Neurodegeneration Associated With Aging',
646 *Front Neurosci*, 12: 470.
- 647 Nair, Anroop B., and Shery Jacob. 2016. 'A simple practice guide for dose conversion between animals and
648 human', *Journal of basic and clinical pharmacy*, 7: 27-31.
- 649 Nutt, D. 2006. 'GABAA receptors: subtypes, regional distribution, and function', *J Clin Sleep Med*, 2: S7-11.
- 650 Otsu, N. 1979. 'A Threshold Selection Method from Gray-Level Histograms', *IEEE Transactions on Systems,*
651 *Man, and Cybernetics*, 9: 62-66.
- 652 Pan, Hongna, Tetsade C. B. Piermartiri, Jun Chen, John McDonough, Craig Oppel, Wafae Driwech, Kristin
653 Winter, Emylee McFarland, Katelyn Black, Taiza Figueiredo, Neil Grunberg, and Ann M. Marini.
654 2015. 'Repeated systemic administration of the nutraceutical alpha-linolenic acid exerts
655 neuroprotective efficacy, an antidepressant effect and improves cognitive performance when
656 given after soman exposure', *Neurotoxicology*, 51: 38-50.
- 657 Patel, V., C. Ramasundarahettige, L. Vijayakumar, J. S. Thakur, V. Gajalakshmi, G. Gururaj, W. Suraweera,
658 and P. Jha. 2012. 'Suicide mortality in India: a nationally representative survey', *Lancet*, 379: 2343-
659 51.
- 660 Pearson, J. N., and M. Patel. 2016. 'The role of oxidative stress in organophosphate and nerve agent
661 toxicity', *Ann N Y Acad Sci*, 1378: 17-24.
- 662 Pereira, E. F., Y. Aracava, L. J. DeTolla, Jr., E. J. Beecham, G. W. Basinger, Jr., E. J. Wakayama, and E. X.
663 Albuquerque. 2014. 'Animal models that best reproduce the clinical manifestations of human
664 intoxication with organophosphorus compounds', *J Pharmacol Exp Ther*, 350: 313-21.
- 665 Pessah, I. N., M. A. Rogawski, D. J. Tancredi, H. Wulff, D. Zolkowska, D. A. Bruun, B. D. Hammock, and P. J.
666 Lein. 2016. 'Models to identify treatments for the acute and persistent effects of seizure-inducing
667 chemical threat agents', *Ann N Y Acad Sci*, 1378: 124-36.
- 668 Phelan, K. D., U. T. Shwe, D. K. Williams, L. J. Greenfield, and F. Zheng. 2015. 'Pilocarpine-induced status
669 epilepticus in mice: A comparison of spectral analysis of electroencephalogram and behavioral
670 grading using the Racine scale', *Epilepsy Res*, 117: 90-6.
- 671 Piermartiri, Tetsade C. B., Hongna Pan, Jun Chen, John McDonough, Neil Grunberg, James P. Apland, and
672 Ann M. Marini. 2015. 'Alpha-Linolenic Acid-Induced Increase in Neurogenesis is a Key Factor in
673 the Improvement in the Passive Avoidance Task After Soman Exposure', *NeuroMolecular Medicine*,
674 17: 251-69.
- 675 Pirker, S., C. Schwarzer, A. Wieselthaler, W. Sieghart, and G. Sperk. 2000. 'GABA(A) receptors:
676 immunocytochemical distribution of 13 subunits in the adult rat brain', *Neuroscience*, 101: 815-50.
- 677 Pope, Carey, Subramanya Karanth, and Jing Liu. 2005. 'Pharmacology and toxicology of cholinesterase
678 inhibitors: uses and misuses of a common mechanism of action', *Environmental Toxicology and*
679 *Pharmacology*, 19: 433-46.
- 680 Pouliot, W., S. L. Bealer, B. Roach, and F. E. Dudek. 2016. 'A rodent model of human organophosphate
681 exposure producing status epilepticus and neuropathology', *Neurotoxicology*, 56: 196-203.
- 682 Reddy, S. D., and D. S. Reddy. 2015. 'Midazolam as an anticonvulsant antidote for organophosphate
683 intoxication--A pharmacotherapeutic appraisal', *Epilepsia*, 56: 813-21.
- 684 Schmued, L. C., C. C. Stowers, A. C. Scallet, and L. Xu. 2005. 'Fluoro-Jade C results in ultra high resolution
685 and contrast labeling of degenerating neurons', *Brain Res*, 1035: 24-31.
- 686 Silbergleit, R., D. Lowenstein, V. Durkalski, and R. Conwit. 2011. 'RAMPART (Rapid Anticonvulsant
687 Medication Prior to Arrival Trial): a double-blind randomized clinical trial of the efficacy of

- 688 intramuscular midazolam versus intravenous lorazepam in the prehospital treatment of status
 689 epilepticus by paramedics', *Epilepsia*, 52 Suppl 8: 45-7.
- 690 ———. 2013. 'Lessons from the RAMPART study--and which is the best route of administration of
 691 benzodiazepines in status epilepticus', *Epilepsia*, 54 Suppl 6: 74-7.
- 692 Siso, S., B. A. Hobson, D. J. Harvey, D. A. Bruun, D. J. Rowland, J. R. Garbow, and P. J. Lein. 2017. 'Editor's
 693 Highlight: Spatiotemporal Progression and Remission of Lesions in the Rat Brain Following Acute
 694 Intoxication With Diisopropylfluorophosphate', *Toxicol Sci*, 157: 330-41.
- 695 Spanpanato, J., W. Pouliot, S. L. Bealer, B. Roach, and F. E. Dudek. 2019. 'Antiseizure and neuroprotective
 696 effects of delayed treatment with midazolam in a rodent model of organophosphate exposure',
 697 *Epilepsia*, 60: 1387-98.
- 698 Ulu, A., B. Inceoglu, J. Yang, V. Singh, S. Vito, H. Wulff, and B. D. Hammock. 2016. 'Inhibition of soluble
 699 epoxide hydrolase as a novel approach to high dose diazepam induced hypotension', *J Clin Toxicol*,
 700 6.
- 701 Valdes Hernandez Mdel, C., L. C. Maconick, E. M. Tan, and J. M. Wardlaw. 2012. 'Identification of mineral
 702 deposits in the brain on radiological images: a systematic review', *Eur Radiol*, 22: 2371-81.
- 703 Wu, X., R. Kuruba, and D. S. Reddy. 2018. 'Midazolam-Resistant Seizures and Brain Injury after Acute
 704 Intoxication of Diisopropylfluorophosphate, an Organophosphate Pesticide and Surrogate for
 705 Nerve Agents', *J Pharmacol Exp Ther*, 367: 302-21.
- 706 Yamamoto, S., M. Suzuki, K. Kohara, G. Iinuma, and N. Moriyama. 2007. 'Technical aspects of X-ray micro-
 707 computed tomography: initial experience of 27-microm resolution using Feldkamp cone-beam
 708 reconstruction', *Nihon Hoshasen Gijutsu Gakkai Zasshi*, 63: 257-60.
- 709 Yamasue, Hidenori, Osamu Abe, Kiyoto Kasai, Motomu Suga, Akira Iwanami, Haruyasu Yamada, Mamoru
 710 Tochigi, Toshiyuki Ohtani, Mark A. Rogers, Tsukasa Sasaki, Shigeki Aoki, Tadafumi Kato, and
 711 Nobumasa Kato. 2007. 'Human brain structural change related to acute single exposure to sarin',
 712 *Annals of Neurology*, 61: 37-46.
- 713 Youssef, S. A., M. T. Capucchio, J. E. Rofina, J. K. Chambers, K. Uchida, H. Nakayama, and E. Head. 2016.
 714 'Pathology of the Aging Brain in Domestic and Laboratory Animals, and Animal Models of Human
 715 Neurodegenerative Diseases', *Vet Pathol*, 53: 327-48.
- 716 Zaja-Milatovic, S., R. C. Gupta, M. Aschner, and D. Milatovic. 2009. 'Protection of DFP-induced oxidative
 717 damage and neurodegeneration by antioxidants and NMDA receptor antagonist', *Toxicol Appl
 718 Pharmacol*, 240: 124-31.
- 719 Zhang, T., M. S. Todorovic, J. Williamson, and J. Kapur. 2017. 'Flupirtine and diazepam combination
 720 terminates established status epilepticus: results in three rodent models', *Ann Clin Transl Neurol*,
 721 4: 888-96.
- 722

723 **Figure legends**

724 **Fig. 1. Experimental paradigm.** (A) Adult male Sprague Dawley rats were pretreated with pyridostigmine
 725 bromide (PB) at 0.1 mg/kg (*i.p.*), and then randomly assigned to vehicle (VEH), DFP, DFP + diazepam (DZP)
 726 or DFP + midazolam (MDZ) groups. Vehicle (saline) or DFP (4 mg/kg, *s.c.*) were administered 30 min after
 727 pyridostigmine bromide, and followed 1 min later by *i.m.* injections of atropine sulfate (AS, 2 mg/kg) and
 728

729 pralidoxime (2-PAM, 25 mg/kg). At 40 min after DFP injection, vehicle (saline), diazepam (5 mg/kg, *i.p.*), or
730 midazolam (0.73 mg/kg, *i.m.*) were administered, and animals were monitored for seizure activity for 4 h. At 3
731 and 6 months post-exposure, animals were imaged using *in vivo* micro-CT prior to euthanasia for
732 neuropathologic assessments, including FluoroJade-C staining and immunohistochemical (IHC) analyses of
733 neuroinflammation. *Three animals were removed from each of the diazepam and midazolam groups for
734 separate analyses not included in this study; thus only 7 animals from these groups moved forward for IHC and
735 micro-CT assessment at 3 and 6 months. (B) Summary of sample sizes used for outcome measures at 3 and 6
736 months post-exposure. A total of 14 vehicle, 14 DFP, 7 diazepam and 7 midazolam animals were available after
737 the acute seizure analyses. At 3 months post-exposure, 4 vehicle, 12 DFP, 6 diazepam and 5 midazolam animals
738 were successfully imaged using micro-CT, and 6 vehicle, 6 DFP, 3 diazepam and 3 midazolam were randomly
739 selected to be euthanized to collect brains for histological analyses, leaving 8 vehicle, 8 DFP, 4 diazepam and 4
740 midazolam animals for the 6 month time point. For the micro-CT studies at 6 months, 7 vehicle, 8 DFP, 4
741 diazepam and 4 midazolam animals were successfully imaged. Following micro-CT imaging, 8 vehicle, 8 DFP,
742 4 diazepam and 4 midazolam animals were euthanized to collect their brains for histological analyses.

743 #Information from both time points were combined across groups for statistical analysis.

744 **Fig. 2. Benzodiazepine pharmacokinetics and pharmacodynamics.** (A) Total diazepam (5 mg/kg, *i.p.*) and
745 midazolam (0.73 mg/kg, *i.m.*) concentrations were measured in the brain and serum of naïve adult male rats at
746 varying times post-administration. Data are presented as the mean \pm S.D. (n=3-4 animals/time point). (B) Effect
747 of diazepam and midazolam on DFP-induced seizure behavior. A modified Racine scale was used to score
748 seizure behavior at 5 min intervals from 0-120 min post-DFP, and at 20-min intervals from 120-240 min post-
749 DFP (≥ 10 observations per animal). The average seizure score was calculated as the time-weighted average of
750 the animal's individual seizure scores across the 4 h of observation. Data presented as the mean \pm S.E.M. (n =
751 10-14 animals/group). *P<0.05 by one-way ANOVA with post-hoc Kruskal-Wallis test.

Fig. 3. DFP causes persistent neurodegeneration that persists at 6 months post-exposure even with benzodiazepine therapy. (A) Representative photomicrographs of FluoroJade C (FJC) staining in the CA1 subregion of the hippocampus at 3 and 6 months post-DFP exposure. Bar = 200 μ m. (B) The number of FJC-labeled cells was quantified in seven brain regions (amygdala, CA1, CA3, and dentate gyrus of the hippocampus, piriform and somatosensory cortex, and thalamus) at 3 and 6 months post-DFP exposure. Estimates of exposure or treatment effects at each time point were averaged across brain regions as the group differences in number of FJC+ cells did not differ significantly between brain regions. Data are presented as the geometric mean ratio with 95% confidence interval (n = 6-8 vehicle, 6-8 DFP, 3-4 diazepam, 3-4 midazolam animals per time point). Confidence intervals that do not include 1.00 are colored blue and indicate a significant difference between groups at $P < 0.05$. Raw data used to generate this figure are provided in the supplemental material (Fig. S1).

Fig. 4. Midazolam but not diazepam attenuates GFAP upregulation in some but not all brain regions. (A) Representative photomicrographs of GFAP immunoreactivity (reactive astrocytes, red) in the thalamus at 6 months post-exposure. Sections were counterstained with DAPI (blue) to label cell nuclei. Bar = 200 μ m. (B) The percent area of GFAP immunoreactivity was quantified in seven brain regions at 3 and 6 months post-DFP exposure. Estimates of exposure or treatment effects by brain region were averaged across time points as group differences did not differ significantly between time points. Data are presented as the geometric mean ratio with 95% confidence intervals (n = 14 vehicle, 14 DFP, 7 diazepam, 7 midazolam animals combined across time points). Confidence intervals that do not include 1.00 are colored blue and indicate a significant difference between groups at $P < 0.05$. Raw data used to generate this figure are provided in the supplemental material (Fig. S2).

Fig. 5. Diazepam and midazolam reduce S100 β immunoreactivity in a region-specific manner. (A) Representative photomicrographs of S100 β immunoreactivity (astrocytes, green) in the CA3 subregion of the hippocampus at 6 months post-exposure. Sections were counterstained with DAPI (blue) to label cell nuclei.

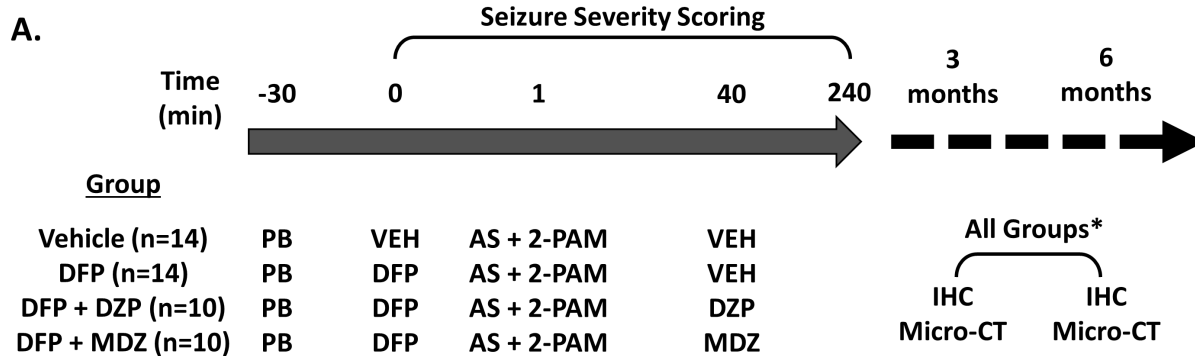
776 Bar = 200 μm . (B) The percent area of S100 β immunoreactivity was quantified in seven brain regions at 3 and 6
777 months post-DFP exposure. Estimates of exposure or treatment effects by brain region were averaged across
778 time point as group differences did not differ significantly between time points. Data are presented as the
779 geometric mean ratio with 95% confidence intervals (n = 14 vehicle, 14 DFP, 7 diazepam, 7 midazolam animals
780 combined across time points). Confidence intervals that do not include 1.00 are colored blue and indicate a
781 significant difference between groups at $P < 0.05$. Raw data used to generate this figure are provided in the
782 supplemental material (Fig. S3).

783 **Fig. 6. Neither diazepam nor midazolam reduce persistent microglial activation.** (A) Representative
784 photomicrographs of IBA-1 (microglia; red) and CD68 (phagocytic microglia; green) immunoreactivity in the
785 thalamus at 6 months post-exposure. Sections were counterstained with DAPI (blue) to label cell nuclei. Bar =
786 200 μm . (B) The percent of total cells that were IBA-1 immunopositive and the percent of IBA-1
787 immunopositive cells that were immunoreactive for CD68 were quantified in seven brain regions (amygdala,
788 CA1, CA3 and dentate gyrus of the hippocampus, piriform and somatosensory cortex, and thalamus) at 3 and 6
789 months post-DFP exposure. Estimates of exposure or treatment effects were averaged across brain regions and
790 time points as these did not differ significantly by brain region or time point. Data are presented as the
791 geometric mean ratio with 95% confidence intervals (n = 14 vehicle, 14 DFP, 7 diazepam, 7 midazolam animals
792 combined across time points). Confidence intervals that do not include 1.00 are colored blue and indicate a
793 significant difference between groups at $P < 0.05$. Raw data used to generate this figure are provided in the
794 supplemental material (Fig. S4 and S5).

795 **Fig. 7. Biomarkers of oxidative stress are not significantly elevated in the brain of DFP-intoxicated**
796 **animals at 3 or 6 months post-DFP exposure.** (A) Representative photomicrographs of NeuN (neurons; red)
797 and 3-nitrotyrosine (oxidative damage; green) immunoreactivity in the CA3 subregion of the hippocampus at 6
798 months post-exposure. Sections were counterstained with DAPI (blue) to label cell nuclei. Bar = 200 μm . (B)
799 The percent of total cells that were immunopositive for NeuN and the percent of NeuN immunopositive cells

800 that expressed 3-nitrotyrosine were quantified in seven brain regions (amygdala, CA1, CA3 and dentate gyrus
801 of the hippocampus, piriform and somatosensory cortex, and thalamus) at 3 and 6 months post-DFP. Estimates
802 of exposure or treatment effects were averaged across brain regions and time points as these did not differ
803 significantly by brain region or time point. Data represented as geometric mean ratio (percent of NeuN
804 immunopositive cells that expressed 3-nitrotyrosine) or estimated differences between groups (percent of total
805 cells that were immunopositive for NeuN) with 95% confidence intervals (n = 14 vehicle, 14 DFP, 7 diazepam,
806 7 midazolam animals combined across time points). Confidence intervals entirely above 1 (percent of NeuN
807 immunopositive cells that expressed 3-NT) or 0 (percent of total cells that were immunopositive for NeuN) are
808 colored blue satisfy $P < 0.05$. Raw data used to generate this figure are provided in the supplemental material
809 (Fig. S6 and S7).

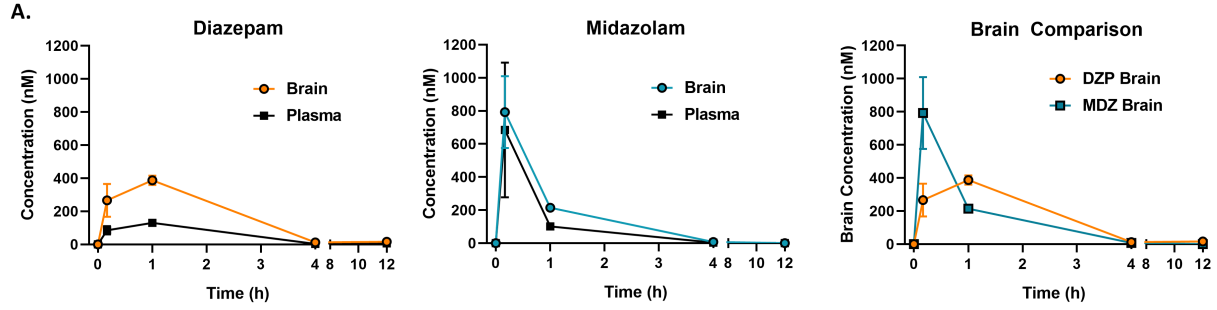
810 **Fig. 8. Neither diazepam nor midazolam protect against delayed DFP-induced mineralization in the**
811 **brain.** (A) Representative micro-CT output images overlaid on anatomical MR images at 6 months post-
812 exposure. Mineralized areas are shown in green, and arrows point to representative mineral deposits. (B)
813 Reconstructed three-dimensional micro-CT images showing the hippocampus (solid blue), thalamus
814 (transparent green), and mineralized area (solid green) at 6 months post-exposure. (C) Quantitative analyses
815 comparing the percent area of mineralization in the dorsolateral (top) and medial (bottom) thalamus at 3 and 6
816 months post-exposure. Data are presented as the geometric mean ratio with 95% confidence intervals (n = 4-7
817 vehicle, 8-12 DFP, 4-7 diazepam, 4-7 midazolam animals per time point; note that a subset of animals were
818 imaged at both 3 and 6 months). Confidence intervals that do not include 1.00 are colored blue and indicate a
819 significant difference between groups at $P < 0.05$. Raw data used to generate this figure are provided in the
820 supplemental material (Fig. S8).



B.

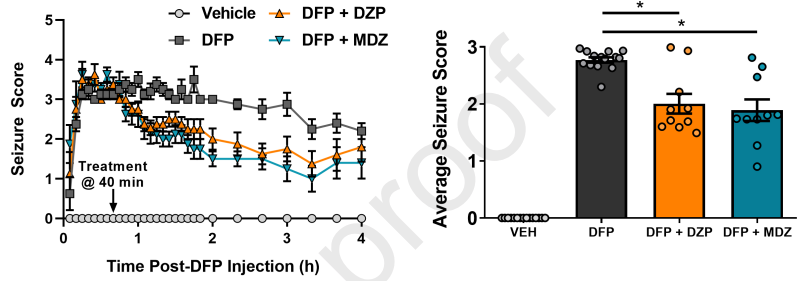
Summary of sample sizes.

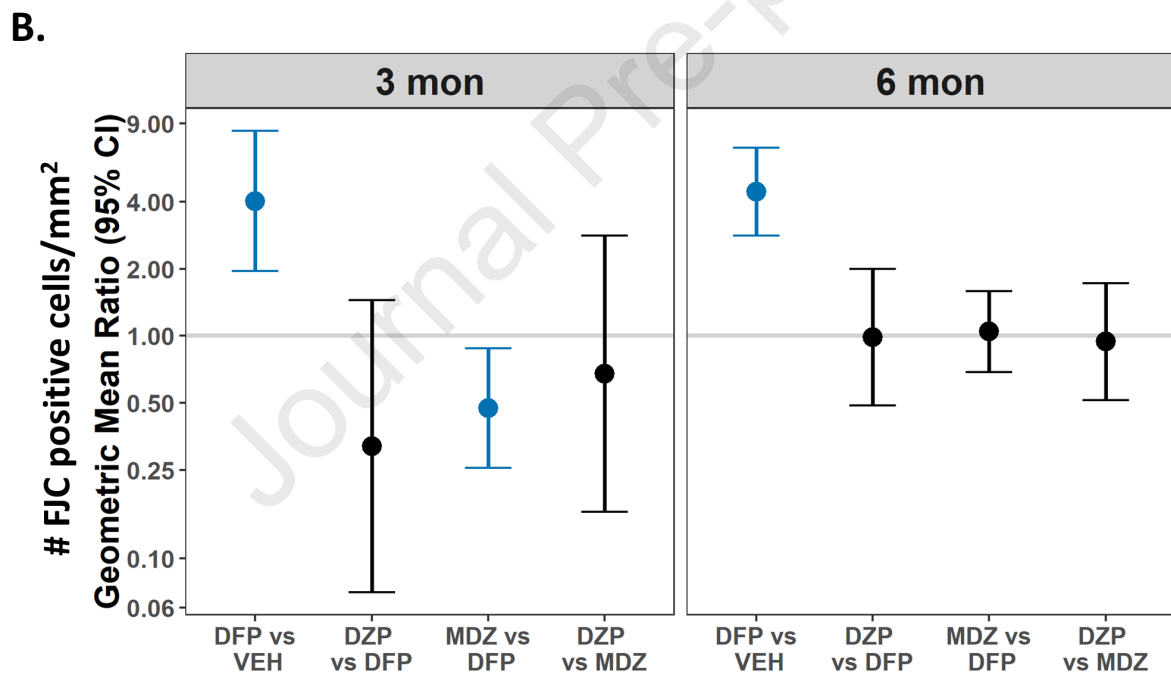
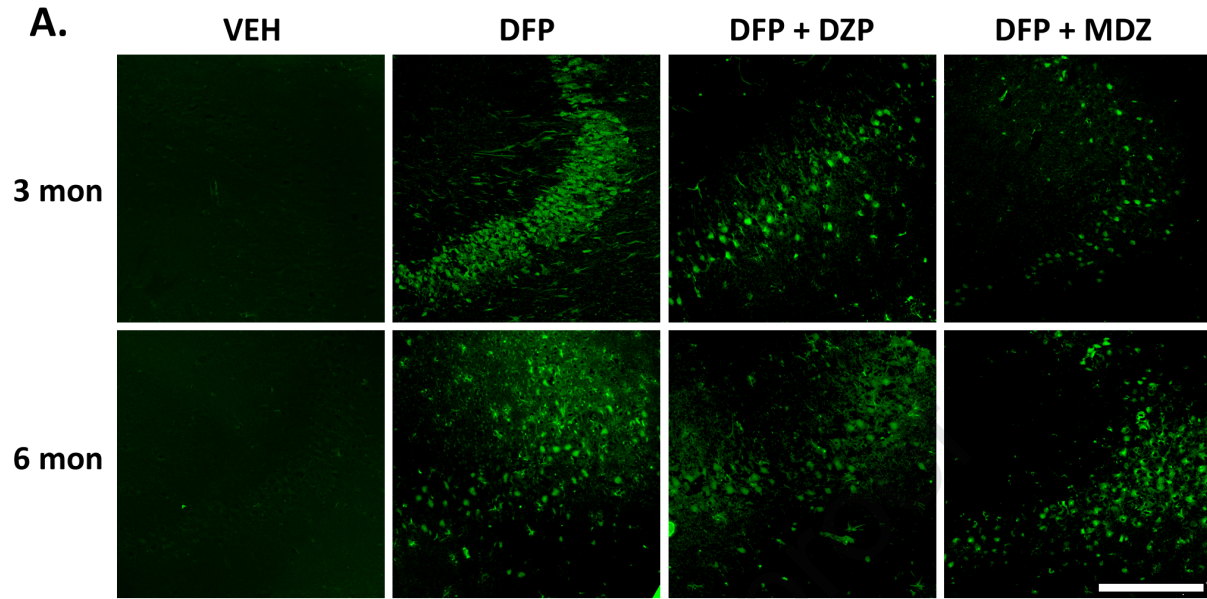
Endpoint(s) Evaluated	Sample Size (3 months)	Sample Size (6 months)	Figure
Fluoro-Jade C (FJC)	6 VEH, DFP 3 DZP, MDZ	8 VEH, DFP 4 DZP, MDZ	3
Immunohistochemistry [#]	6 VEH, DFP 3 DZP, MDZ	8 VEH, DFP 4 DZP, MDZ	4-7
Micro-CT	4 VEH, 12 DFP 6 DZP, 5 MDZ	7 VEH, 8 DFP 4 DZP, 4 MDZ	8

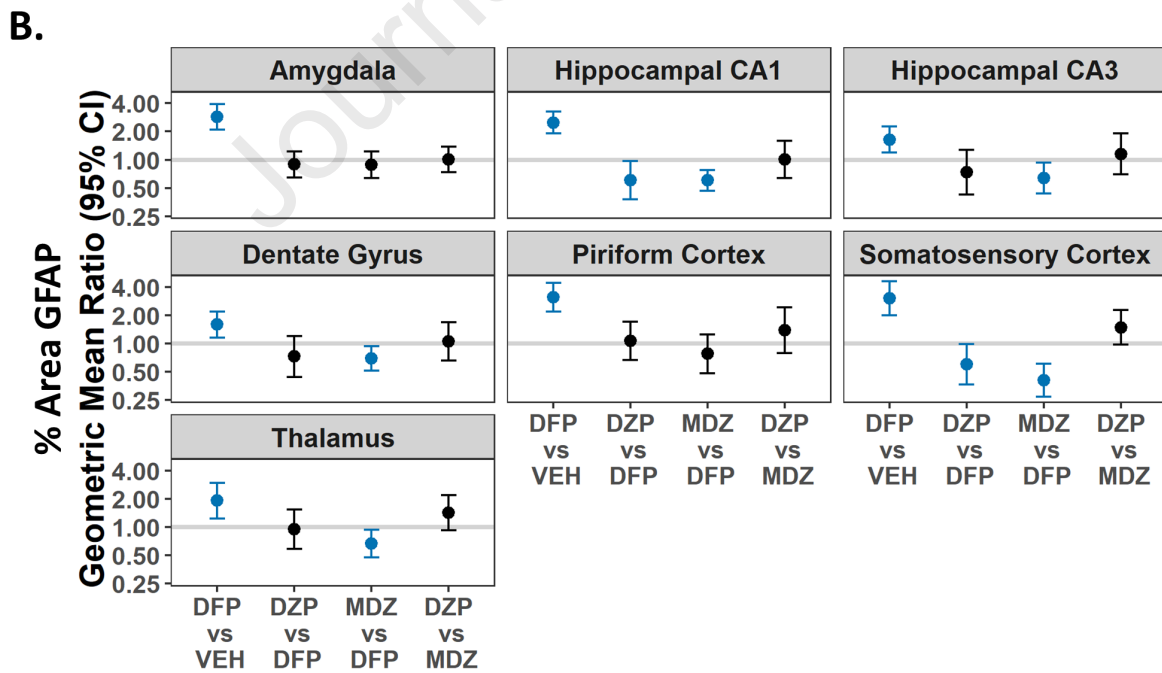
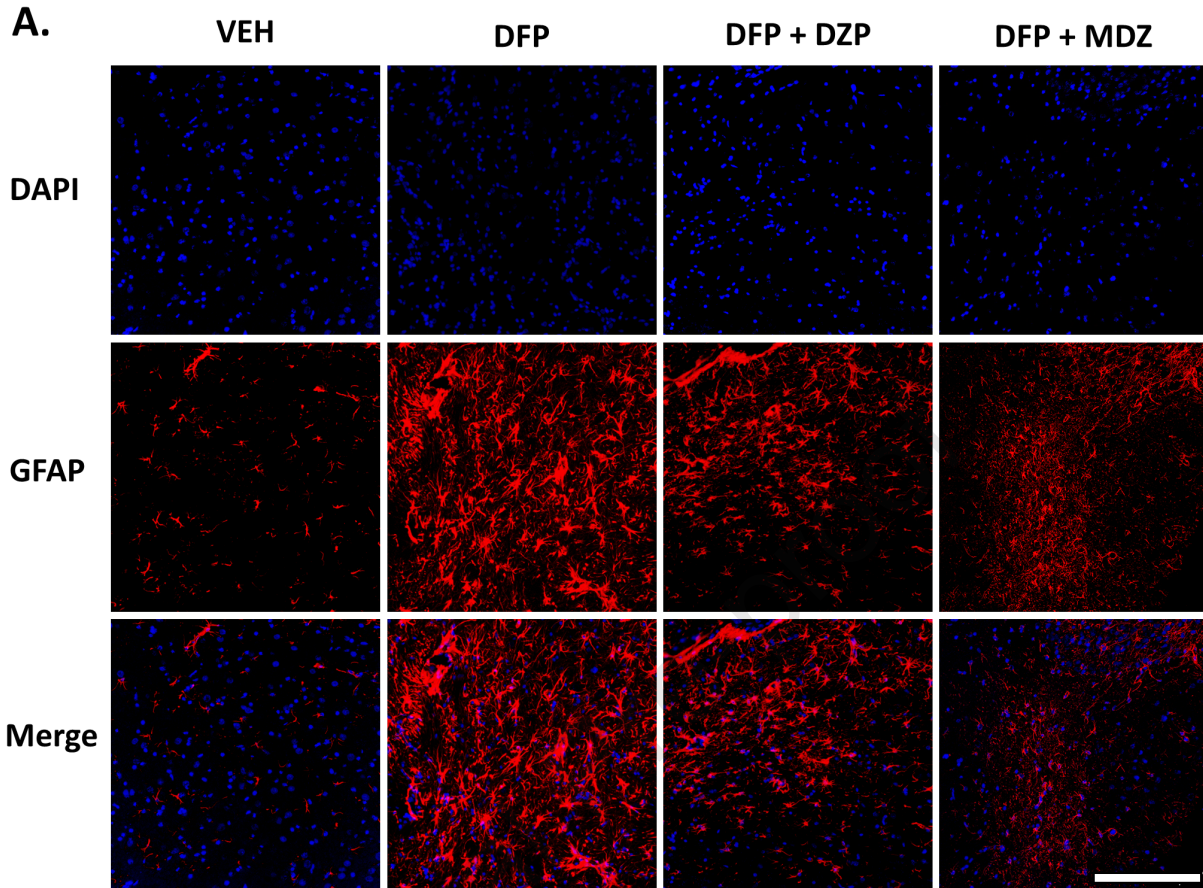


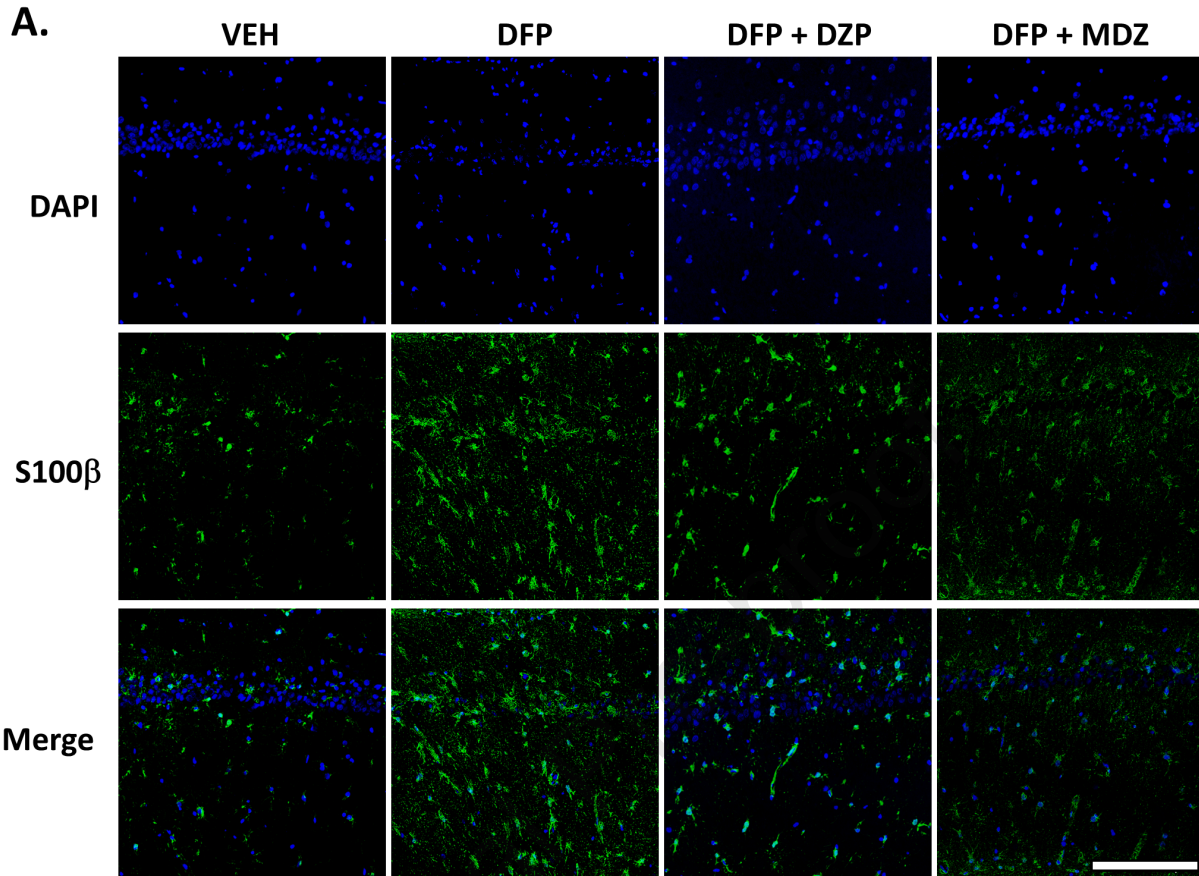
B.

Score	Behavior
0	No behavioral abnormalities
1	SLUD
2	Tremors, Muscle Fasciculations
3	Forelimb Clonus
4	Rearing, Hindlimb Clonus
5	Falling, Loss of Righting Reflex

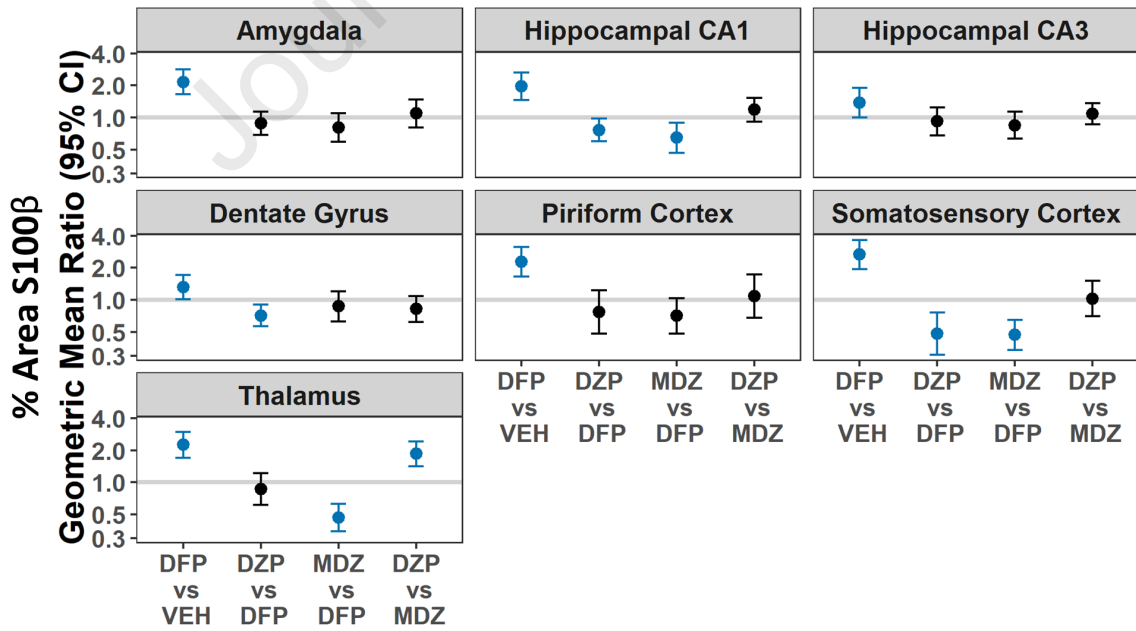


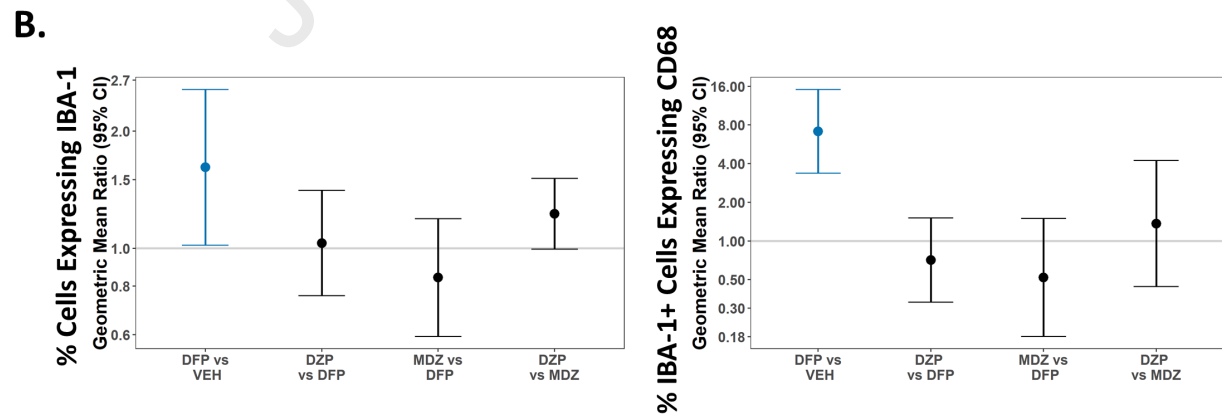
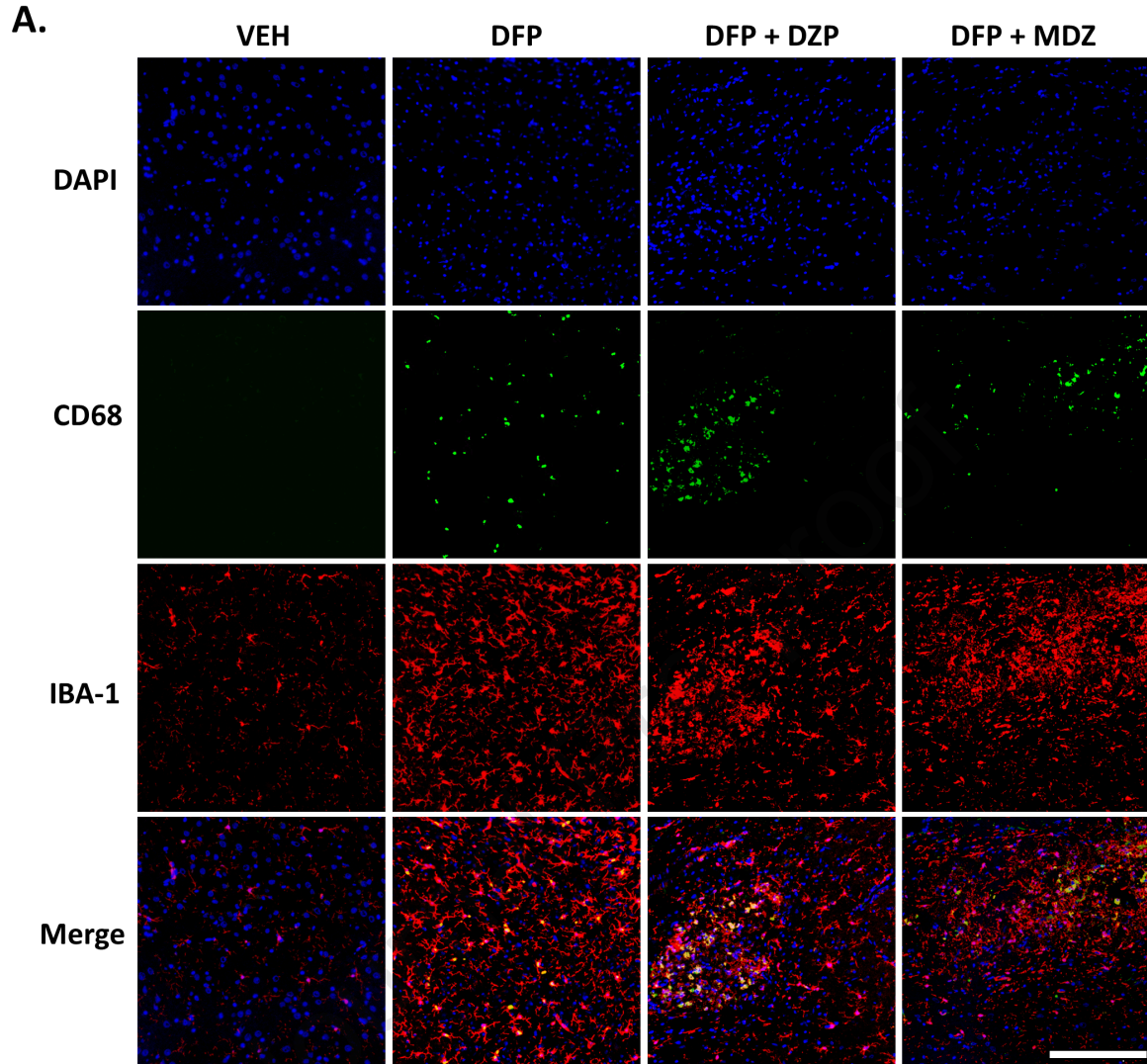




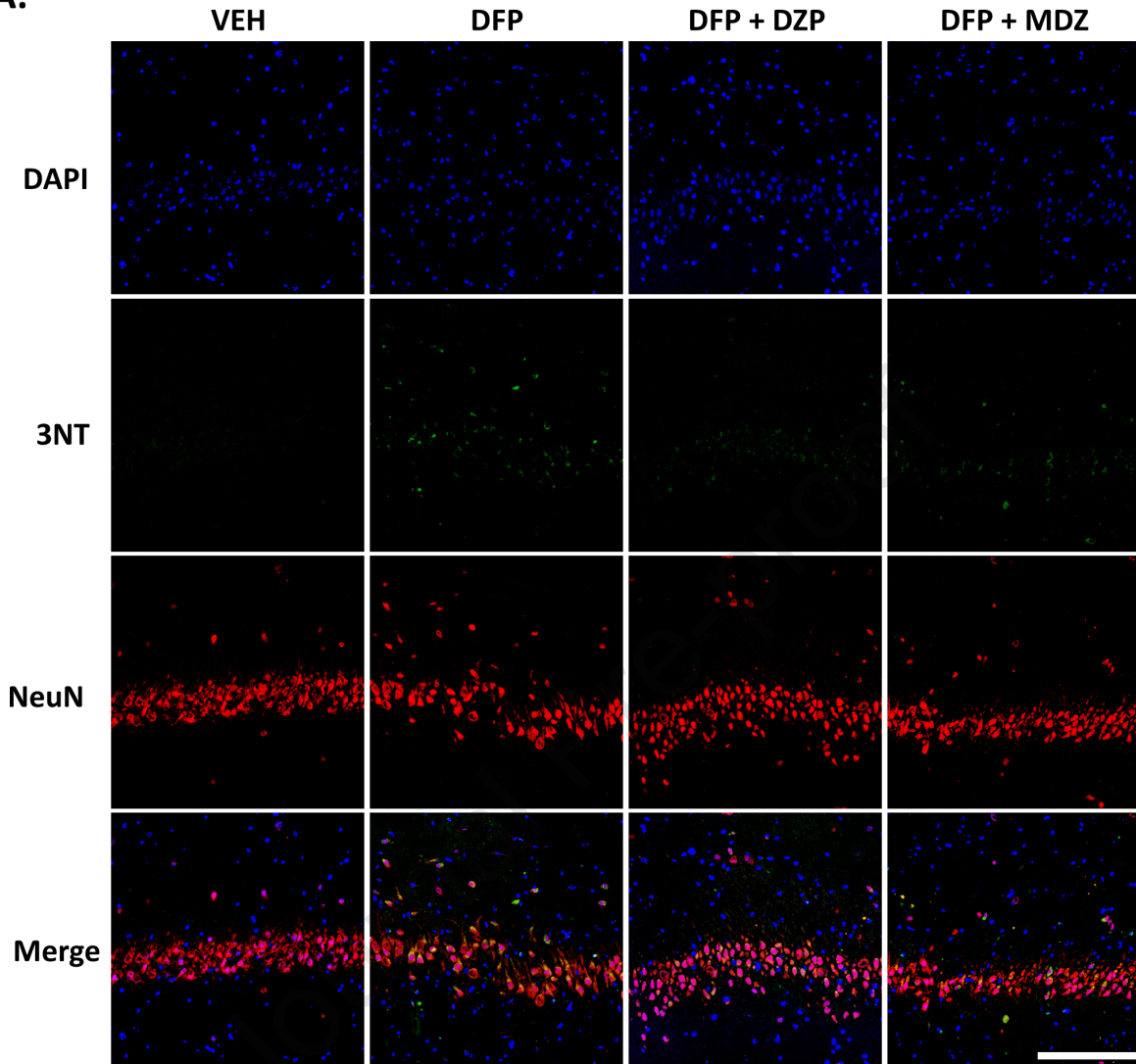


B.

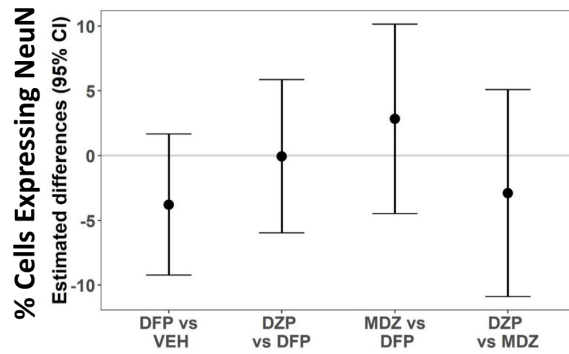




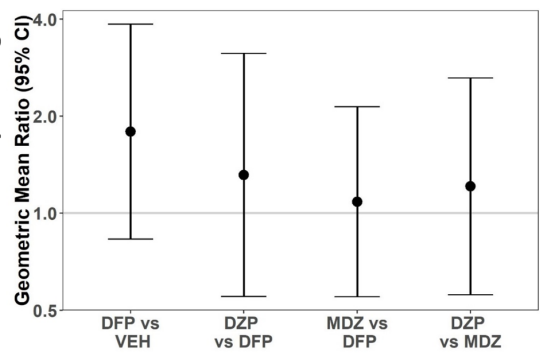
A.

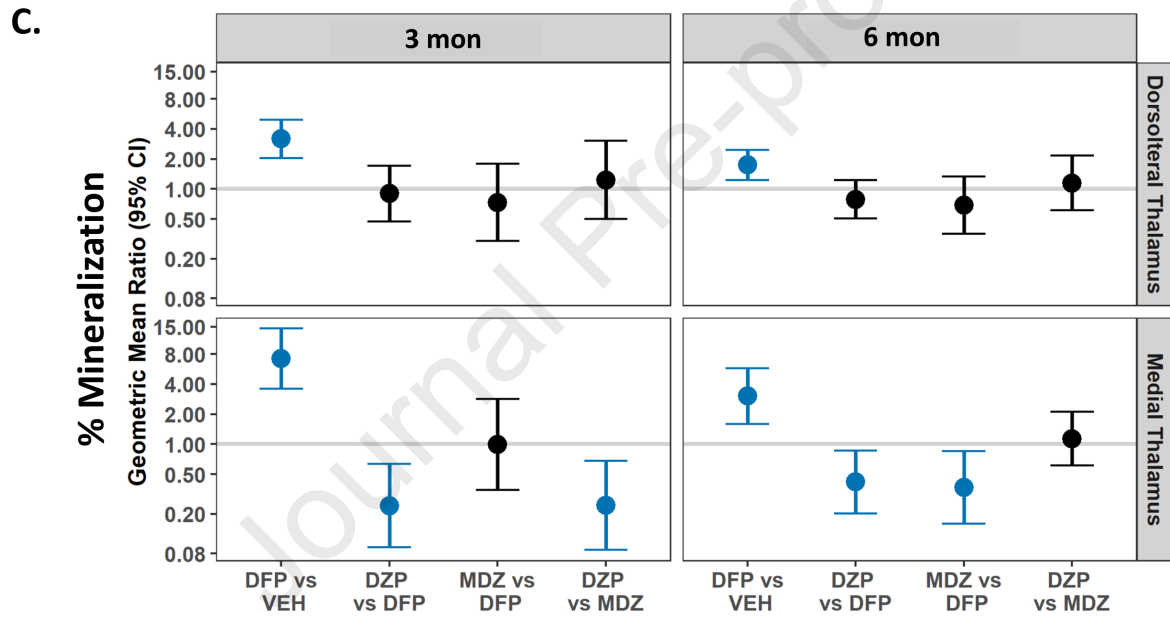
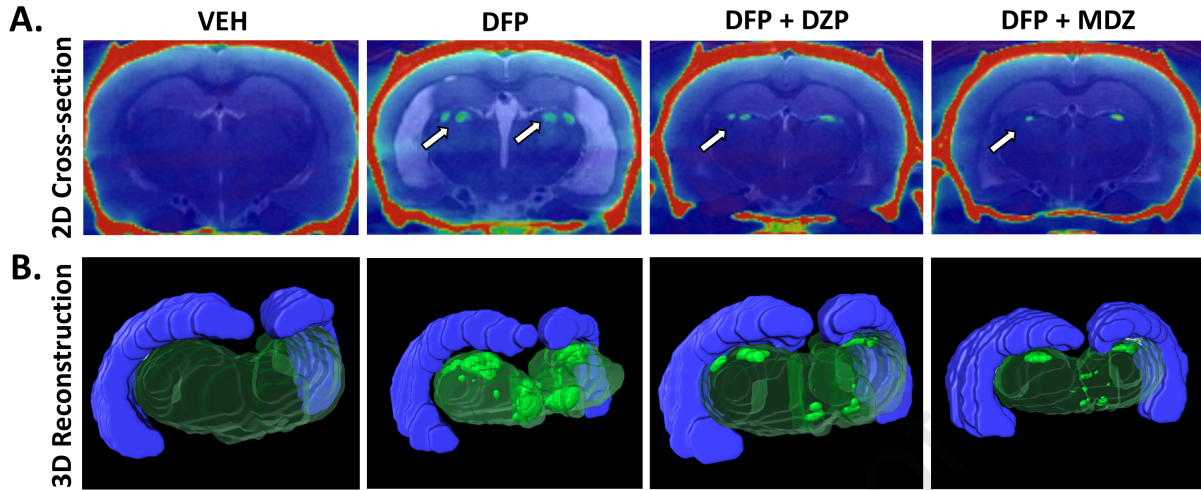


B.



% NeuN+ Cells Expressing 3NT





Highlights:

- Human survivors of acute OP intoxication exhibit long-term neurological sequelae
- Current standard of care does not prevent long-term effects of acute OP intoxication
- Neuroinflammation is a potential therapeutic target for improving patient outcomes

Journal Pre-proof